Chapter 11
Lean NOx Reduction by NH_3 on Fe-Exchanged Zeolite and Layered Fe/Cu Zeolite Catalysts: Mechanisms, Kinetics, and Transport Effects

Michael P. Harold and Pranit Metkar

11.1 Introduction

Rising transportation fuel costs have increased the use of diesel-powered vehicles, which are more fuel efficient than their gasoline counterparts. But the lean diesel exhaust contains NOx ($NO + NO_2$) which is notoriously difficult to reduce in the presence of excess O_2. Selective catalytic reduction (SCR) of NOx with NH_3 generated from onboard hydrolysis of urea has emerged as the catalytic process of choice for reduction of NOx from the exhaust of medium- and heavy-duty vehicles and engines. Various catalysts have been studied and researched for ammonia-based SCR. The earlier success of Vanadia-based catalysts, such as $V_2O_5/WO_3/TiO_2$ for stationary source applications, has led to their study for mobile applications [1–8]. However, while the V-based catalyst has very good selectivity to N_2 at temperatures below 500 °C, the catalyst suffers from significant deactivation at higher temperatures that may be encountered during driving conditions. Moreover, the catalyst is volatile at higher temperatures which could lead to the undesirable release of V species. For these reasons, recent research has focused on Fe- and Cu-based zeolite catalysts which are found to have high NO_x activity and selectivity over a wide range of temperatures [9–12]. The performance of Cu- and Fe-zeolite catalysts has been reported in [13–27], respectively. In general, Cu-based catalysts have higher activity at lower temperatures (<300 °C) whereas Fe-based catalysts are more active at higher temperatures (>350 °C). BASF has commercialized the eight-membered ring, small pore Cu-exchanged chabazite zeolite, originally

M. P. Harold (✉) · P. Metkar
Department of Chemical and Biomolecular Engineering, University of Houston, 4800 Calhoun Road, Houston, TX 77204, USA
e-mail: mharold@uh.edu

P. Metkar
DuPont Company, Central Research and Development, Wilmington, DE 19880, USA

I. Nova and E. Tronconi (eds.), *Urea-SCR Technology for deNOx After Treatment of Diesel Exhausts*, Fundamental and Applied Catalysis,
DOI: 10.1007/978-1-4899-8071-7_11,

discovered by Zones [28]. This catalyst has excellent thermal durability and hydrocarbon tolerance [29, 30]. A related catalyst, Cu-modified SAPO-34, was commercialized during the same period by Johnson-Matthey [31].

The NH_3-based SCR reaction system involves several overall reactions which we identify in the next section. In order to design new catalysts, it is advantageous to understand the workings of existing Fe-based catalysts. This includes the mechanism and kinetics of the main reactions, potential differences in the composition and structure of catalysts, the influence of transport processes, monolith reactor features and performance, among other factors. To this end, our objective for this chapter is to provide an overview of Fe-exchanged zeolite SCR which spans catalyst, kinetics, and reactor features. We do not delve into detail about the catalyst structure and related matters; these were amply covered in a review by Brandenberger et al. [32] a few years ago. Nor do we get into the detail of SCR reactor modeling; this subject was well covered by a review in the same year by Guthenke et al. [33]. Instead, we present representative kinetics and reactor performance data for the SCR reaction system on Fe-exchanged zeolites. Some of the data are either previously unpublished or are taken from the recent literature. Based on these data, the latest views of the SCR mechanism are discussed and corresponding mechanistic-based kinetic models are compared and contrasted. Recent studies investigating the effect of transport processes on the apparent reaction kinetics and reactor behavior are highlighted as well as recently developed catalysts that combine Fe with another metal such as Cu. Finally, we describe the features and predictive capabilities of SCR monolith reactor models that contain kinetic descriptions of varying complexity together with the applicable transport processes.

11.2 Reaction System Performance Features

Bench-scale flow reactor experiments are an effective way of examining the main performance features of the SCR reaction system on various catalysts. In this section, we review these features for Fe-based catalysts as a backdrop to considering more fundamental kinetics and mechanistic studies in Sect. 11.3 and transport effects in Sect. 11.4. The selective catalytic reduction of NOx by ammonia on Fe-ZSM-5 catalyst has been studied in detail by various research groups [19–22, 26, 27, 34–42]. The results from earlier studies of vanadia-based catalysts have underpinned the more recent studies of zeolite-based catalysts. For example, Koebel et al. [3, 6, 43] carried out a detailed study of the SCR chemistry on V-based catalysts. Nova et al. [5, 8, 44, 45] studied the chemistry of SCR over V-based catalyst and proposed a mechanism for the fast SCR reaction. To this end, the data here are by no means unique but are intended to highlight the important trends.

The selective catalytic reduction of gas mixtures containing NO and NO_2 is a complex system involving multiple simultaneous reactions. In order to develop new catalysts and more efficient SCR converters, knowledge of the main reaction

system features and underlying kinetics is essential. Representative performance data presented later in this section are interpreted with the main global reactions in mind. To this end, the selective catalytic reduction of NO/NO_2 by NH_3 involves following three main reactions that lead to the desired N_2 product:

- *Standard SCR Reaction*: This reaction involves NO and NH_3 reacting in presence of O_2: (The heat of the reaction is estimated using standard heats of formation of the reacting and product species with H_2O in gaseous form.)

$$\text{R1: } 4NH_3 + 4NO + O_2 \rightarrow 4N_2 + 6H_2O \qquad \Delta H = -407 \times 10^3 \text{J/mol}NH_3$$

- *Fast SCR Reaction:* When both NO and NO_2 in the feed react simultaneously to produce N_2 and H_2O; it is called as "fast SCR" reaction (2) because it is much faster than the standard SCR reaction (1):

$$\text{R2: } 2NH_3 + NO + NO_2 \rightarrow 2N_2 + 3H_2O \qquad \Delta H = -378 \times 10^3 \text{J/mol}NH_3$$

- *NO_2 SCR Reaction:* This involves the reaction between NO_2 and NH_3 and unlike the standard and fast SCR reactions it has a 4:3 NH_3:NO_2 stoichiometry:

$$\text{R3: } 4NH_3 + 3NO_2 \rightarrow 3.5N_2 + 6H_2O \qquad \Delta H = -341 \times 10^3 \text{J/mol } NH_3$$

Along with the three desired N_2-selective reactions, a number of side reactions occur which result in the undesired consumption of NH_3 or generation of by-products other than N_2, principally N_2O, NH_4NO_3, and HNO_3. NH_3 oxidation is an important side reaction occurring at temperature exceeding 350 °C on Fe-based catalysts. This reaction is undesired since it competes with the selective SCR reactions for the reductant ammonia. On the Fe-zeolite catalysts, NH_3 is selectively oxidized to N_2 by:

$$\text{R4: } 4NH_3 + 3O_2 \rightarrow 2N_2 + 6H_2O \qquad \Delta H = -312 \times 10^3 \text{J/mol } NH_3$$

On the other hand, the oxidation of NO to NO_2 occurs in the temperature range of interest ($T > 150$ °C):

$$\text{R5: } NO + {}^1/_2O_2 \longleftrightarrow NO_2 \qquad \Delta H = -57 \times 10^3 \text{J/mol NO}$$

This reaction is desirable because NO_2 is more effectively reduced by NH_3 than is NO. The existence of NO_2 complicates the reaction system. In particular, the net formation of ammonium nitrate occurs at lower temperatures (ca. 275 °C) as described in detail later:

$$\text{R6: } 2NH_3 + 2NO_2 \rightarrow N_2 + NH_4NO_3 + H_2O$$
$$\Delta H = -291 \times 10^3 \text{J/mol } NH_3$$

Mechanisms involving ammonium nitrate are described in several papers [3, 4, 8, 19, 27, 46, 47]. Koebel and coworkers [1, 3, 4] showed that the first step in this chemistry is NO_2 dimerization

$$\text{R7: } 2NO_2 \longleftrightarrow N_2O_4 \qquad \Delta H = -29.6 \times 10^3 \text{J/mol } N_2O_4$$

The N_2O_4 thus formed reacts with water to form nitrous and nitric acids

$$\text{R8: } N_2O_4 + H_2O \longleftrightarrow HONO + HNO_3 \qquad \Delta H = +18.0 \times 10^3 \text{J/mol } N_2O_4$$

HONO and NH_3 further react to form ammonium nitrite which is unstable above 100 °C, decomposing to N_2 and H_2O

$$\text{R9: } NH_3 + HONO \longleftrightarrow [NH_4NO_2] \rightarrow N_2 + H_2O \qquad \Delta H = -358 \times 10^3 \text{J/mol } NH_3$$

The formation of NH_4NO_3 can also occur by the reaction between NH_3 and HNO_3

$$\text{R10: } NH_3 + HNO_3 \longleftrightarrow NH_4NO_3 \qquad \Delta H = -184 \times 10^3 \text{J/mol } NH_4NO_3$$

The reduction of nitrates by NO has been proposed to be a rate-determining step in the fast SCR chemistry for V-based catalysts [5, 48]:

$$\text{R11: } NH_4NO_3 + NO \rightarrow NO_2 + N_2 + 2H_2O \qquad \Delta H = -175 \times 10^3 \text{J/mol } NH_4NO_3$$

$$\text{R12: } HNO_3 + NO \longleftrightarrow NO_2 + HONO \qquad \Delta H = -1.5 \times 10^3 \text{J/mol } HNO_3$$

This was later confirmed for Fe-based zeolite catalysts by Grossale et al. [27] and Iwasaki et al. [26]. The importance of nitrate reduction was independently revealed by Yeom et al. [49].

Ammonium nitrate decomposes to N_2O at higher temperatures (≥200 °C):

$$\text{R13: } NH_4NO_3 \rightarrow N_2O + 2H_2O \qquad \Delta H = -36.6 \times 10^3 \text{J/mol } NH_4NO_3$$

N_2O is a greenhouse gas and therefore is an undesired by-product and is expected to be controlled in the coming years. N_2O formation also occurs by the overall reaction

$$\text{R14: } 4NH_3 + 4NO_2 + O_2 \rightarrow 4N_2O + 6H_2O \qquad \Delta H = -268 \times 10^3 \text{J/mol } NH_3$$

The N_2O decomposes to N_2 and O_2 at higher temperatures:

$$\text{R15: } 2N_2O \rightarrow N_2 + O_2 \qquad \Delta H = -82 \times 10^3 \text{J/mol } N_2O$$

Finally, Devadas et al. [34] studied the fate of N_2O on Fe-ZSM-5. They observed that ammonia may react with N_2O according to

$$\text{R16: } 2NH_3 + 3N_2O \rightarrow 4N_2 + 3H_2O \qquad \Delta H = -440 \times 10^3 \text{J/mol } N_2O$$

11.2.1 NO Oxidation and NO_2 Decomposition

The NO oxidation reaction has been studied by a number of groups, earlier for V-based catalysts by Suárez et al. [50] and more recently for Fe- and Cu-based catalysts. As mentioned above, the formation of NO_2, when the feed is devoid of NO_2, has been considered an important overall reaction in the SCR system. Earlier studies argued that NO oxidation to NO_2 is an important if not rate-determining step for standard SCR [20, 51, 52]. Metkar et al. [42] suggested, consistent with similar proposals from others for Fe [26] and Cu [53], that the formation of adsorbed NO_2 is the rate-determining step. More recently, Tronconi et al. [54] proposed that NO oxidation to gaseous NO_2 is not the rate-determining step based on a comparison of its rate to that of standard SCR in the absence and presence of H_2O over Fe- and Cu-based zeolites. Schwidder et al. [21] also argued that the formation of gas phase NO_2 cannot be the rate-determining step for standard SCR over Fe-zeolites. This debate about the mechanism encourages a detailed evaluation of the reaction and differences in the activities of various SCR catalysts over a range of conditions. Here we highlight the main features on a commercial Fe-zeolite and synthesized (at UH) Fe-ZSM-5 monolithic catalyst.

NO oxidation displays a distinct maximum in conversion as a function of temperature (Fig. 11.1a). The reaction is kinetically limited up to about 300 °C, beyond which it becomes equilibrium limited due to NO_2 decomposition, a trend that is well-known in the Pt-catalyzed system [55]. The reaction is significantly inhibited by the large excess of H_2O found in exhaust streams. Specifically, when water is added to the mixture of NO and O_2 the rate of NO_2 production drops precipitously. Figure 11.1a shows up to a 90 % drop in the NO conversion over a range of temperatures. The importance of the reverse reaction is seen in Fig. 11.1b, which shows the conversion of NO_2 by decomposition as a function of temperature. These data reveal that the decomposition commences at about 300 °C and becomes more pronounced at higher temperatures, with about 85 % of the NO_2 decomposed by a temperature of 550 °C. The decomposition, like the forward reaction, is significantly inhibited by H_2O. Experiments with a feed mixture of NO, NO_2, and O_2 show the decomposition commencing at a somewhat higher temperature (350 °C in the data shown in Fig. 11.2a reported by Metkar et al. [56]). A focused experiment was carried out to examine more closely the effect of the product NO_2 on the NO oxidation conversion through the incremental addition of NO_2 to a NO + O_2 feed mixture. Figure 11.2b shows a decrease in the conversion with added NO_2 at temperatures in which the rate of NO_2 decomposition was negligible. The dependence reveals that the conversion is a decreasing function of supplemental NO_2, showing that NO_2 inhibits the NO oxidation. We return to this point later.

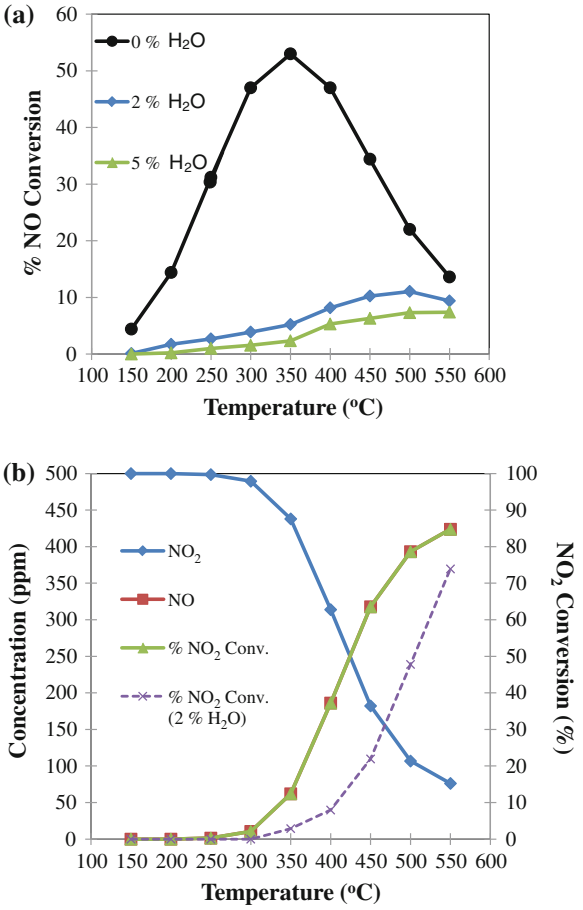

Fig. 11.1 **a** Steady-state conversion of NO versus catalyst temperature during the NO oxidation for different H_2O feed concentrations. Inlet feed: 500 ppm NO, 5 % O_2, 0 or 2 or 5 % H_2O. Total flow: 1,000 sccm, Balance gas: Ar. **b** Steady-state conversion of NO_2 versus catalyst temperature during its decomposition. Feed: 500 ppm NO_2, 0–2 % H_2O. Total flow: 1,000 sccm. Space velocity: 57,000 h^{-1}. Balance gas: Ar. (Adapted from Metkar et al. [42] and used with permission.)

11.2.2 NH_3 Oxidation

The oxidation of NH_3 occurs on Fe-exchanged catalysts and contributes to less than 100 % conversion of NOx at high temperature due to the consumption of the reductant. Figure 11.3 compares a commercial Fe-zeolite catalyst with an as-synthesized Fe-ZSM-5 catalyst (18 wt.% washcoat loading) in the absence of water in the feed. The two catalysts give nearly identical results. The addition of 2 % H_2O in the feed leads to a modest decrease in the NO conversion for the commercial catalyst. As we show later, this modest Fe activity can be exploited in dual component SCR catalyst formulations in which the other metal (Cu) is a much more active ammonia oxidation catalyst.

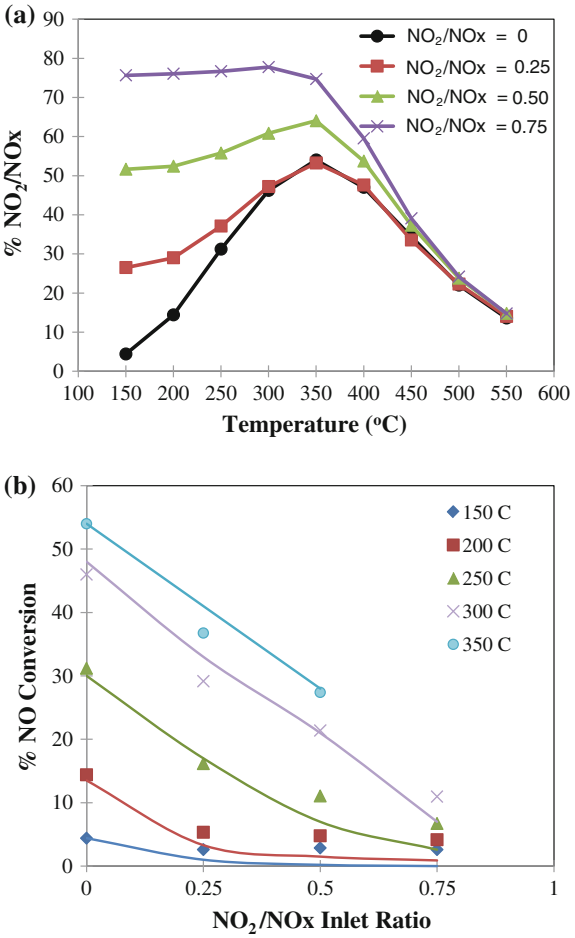

Fig. 11.2 **a** Steady-state outlet NO_2/NOx concentration ratio versus temperature during the NO oxidation reaction with several different feed compositions Inlet feed: 500 ppm NOx (NO + NO_2), 5 % O_2. Total flow: 1,000 sccm. Balance gas: Ar. **b** Steady-state NO conversion during NO oxidation versus NO_2/NOx feed ratio for several temperatures. (Adapted from Metkar et al. [56] and used with permission.)

11.2.3 Selective Catalytic Reduction of NOx

The selective catalytic reduction of NOx by ammonia on Fe-zeolite catalysts displays interesting performance trends over a range of temperatures and NO/NO_2 feed ratios. Feeds containing various NO_2/NOx inlet ratios (0–1) provide insight into the effect of NO_2 which can be appreciable on Fe-exchanged catalysts.

The features of the standard SCR reaction (R1) system (feed devoid of NO_2) are first highlighted. A typical temperature sweep experiment (Fig. 11.4a) shows the changes in the effluent concentrations as a function of temperature when a dry feed containing equal concentrations of NO and NH_3 (NO = NH_3 = 500 ppm) in excess O_2 was passed over an Fe-ZSM-5 catalyst. Negligible NO conversions (<20 %) were observed up to 250 °C. At a temperature of about 300 °C there is a nonlinear increase in NO conversion, which approaches 91 % at 450 °C. The NH_3

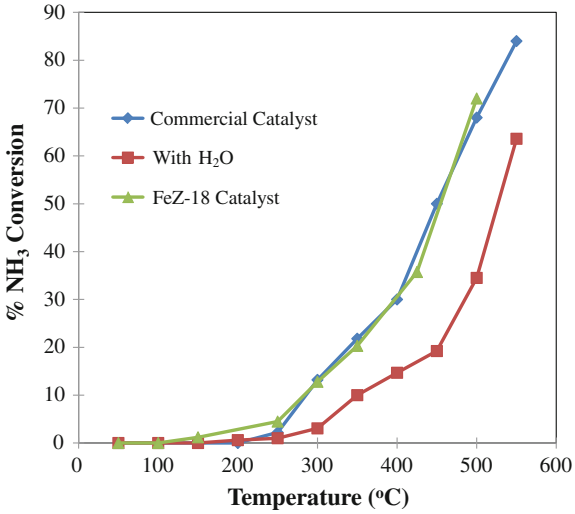

Fig. 11.3 Comparison of the steady-state ammonia converted during the ammonia oxidation on commercial and FeZ-18 catalysts. Effect of water on ammonia oxidation reaction is studied on the commercial catalyst. Feed: 500 ppm NH_3, 5 % O_2, and 0 or 2 % water. Total flow rate: 1,000 sccm. Balance gas: Ar. (Adapted from Metkar et al. [42] and used with permission.)

conversion always exceeds the NO conversion (for $T \geq 300$ °C) because of the aforementioned NH_3 oxidation side reaction. A negligible N_2O yield (<10 ppm) was observed in the temperature range of 250–300 °C. When H_2O was added (2 %) there was only a negligible decrease in the NO conversion (Fig. 11.4b), unlike the much larger effect of H_2O for the oxidations of both NO and NH_3 on the same catalyst. We return to this difference later as it provides clues about the SCR mechanism.

The addition of NO_2 to the feed leads to significant changes in the reactant conversions and product distribution. Figure 11.5a shows the results obtained when a NO_2/NOx feed ratio of 0.25 (total NOx concentration and NH_3 both at 500 ppm) in the presence of 5 % O_2 and no H_2O is contacted on the FeZSM-5 catalyst. It is interesting to note that the apparent NO_2 conversion is essentially complete for the entire temperature range. A substantial increase in the NOx conversion is encountered at lower temperatures compared to that of the standard SCR reaction, and N_2 is the only N-containing product under these conditions. The N-balance is satisfied over the entire temperature range which rules out the formation of any undetected by-products like ammonium nitrate. (We return to this issue later.). A stoichiometric consumption (1:1) of NOx and NH_3 is observed up to 250 °C; beyond this point the ammonia consumption exceeds the NOx conversion due to the ammonia oxidation side reaction, although the difference does not exceed 20 ppm. This parasitic NH_3 oxidation has been observed in other studies and is thought to be a result of an enhancing effect of NOx on the ammonia oxidation that would otherwise not be encountered. In contrast to the standard SCR results, these data indicate that the ammonia oxidation side reaction is less detrimental to the overall NOx conversion in the presence of NO_2. A negligible production of N_2O and complete conversion of NO_2 occurred at all temperatures. The amount of NO consumed is comparable to the amount of NO_2 consumed up to

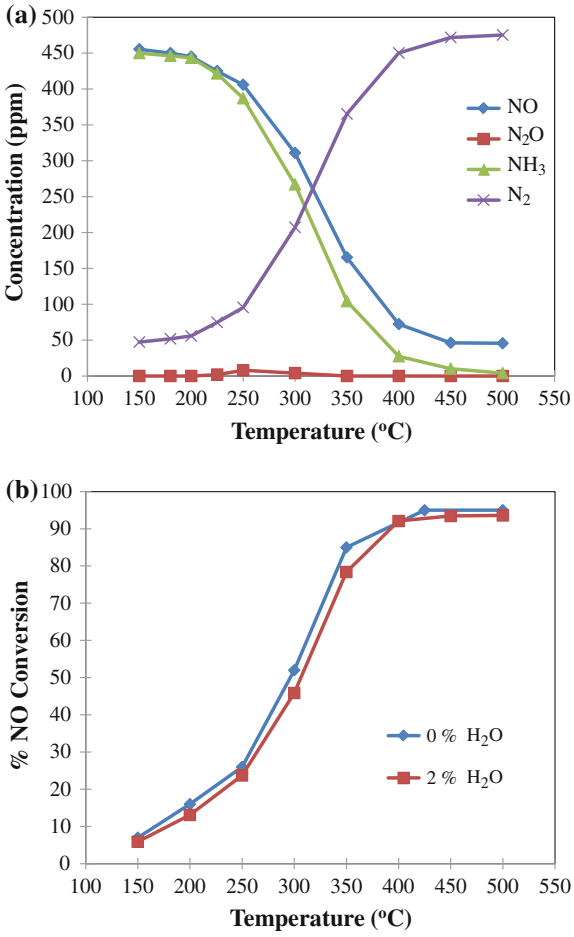

Fig. 11.4 **a** Steady-state product distribution versus temperature for standard SCR on commercial Fe-zeolite catalyst. Space velocity 57,000 h^{-1}. Total Flow rate = 1,000 sccm. Balance gas: Ar. Feed: 500 ppm NO, 500 ppm NH_3, 5 % O_2. **b** Effect of water on standard SCR reaction carried out on the commercial Fe-zeolite catalyst. Inlet feed: 500 ppm NH_3, 500 ppm NO, 5 % O_2, and 0 or 2 % H_2O. Total flow: 1,000 sccm. Balance gas: Ar. (Used with permission [42].)

225 °C. The consumption of equimolar amounts of NO and NO_2 suggests that the fast SCR reaction is the main reaction taking place at these low temperatures and is therefore much faster than the standard SCR reaction. At temperatures above 250 °C, an additional quantity of NO is consumed due to the increase in the standard SCR reaction rate. Finally, although not shown here, when water was added to the feed (2 %), it was found to have only a negligible effect on NOx conversions at most of the temperatures.

When the feed contains equal amounts of NO and NO_2, this corresponds to the stoichiometry of the fast SCR reaction (R2). Typical results obtained for Fe-ZSM-5 catalyst are shown in Fig. 11.5b using a feed devoid of H_2O. The chemistry proceeds much faster than the standard SCR reaction. Very high NOx conversion is obtained at temperatures as low as 180 °C; e.g., a NOx conversion of 74 % was obtained at 180 °C. N_2 is the main product of this reaction with a negligible

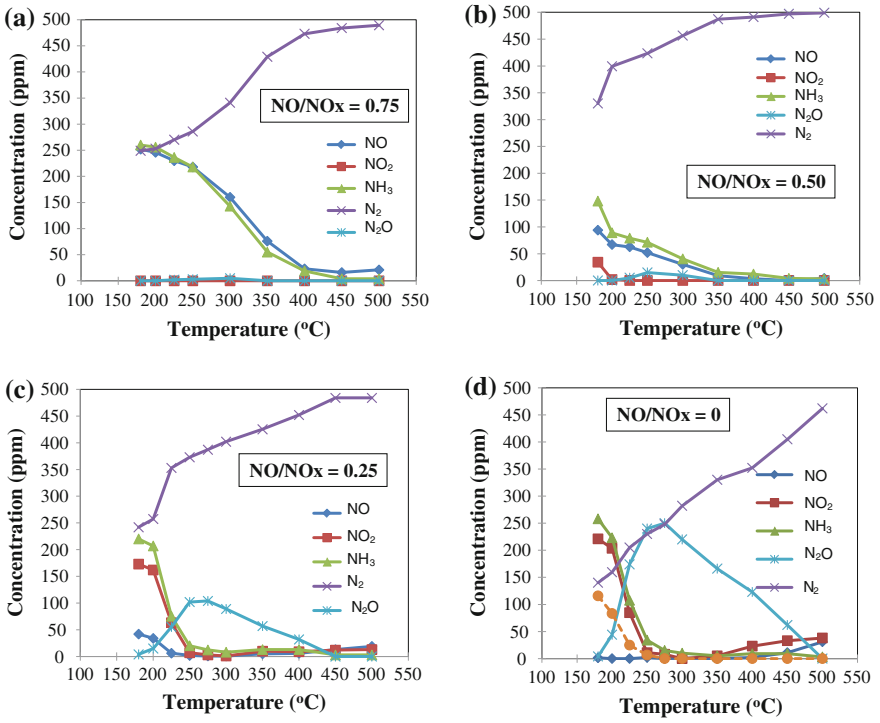

Fig. 11.5 Steady-state product distribution obtained for SCR of NOx with NH_3 as a function of temperature. Space velocity 57,000 h^{-1}. Total Flow rate = 1,000 sccm. Balance gas: Ar. Feed: 500 ppm NH_3, 5 % O_2. **a** 375 ppm NO, 125 ppm NO_2; **b** 250 ppm NO, 250 ppm NO_2; **c** 125 ppm NO, 375 ppm NO_2; **d** 0 ppm NO, 500 ppm NO_2

amount of N_2O (<20 ppm) obtained in the 250–300 °C range. Ammonia is consumed in nearly equimolar amounts as that of NOx. This suggests that the oxidation of ammonia by O_2 is not as important as it is for standard SCR. Similar trends for the fast SCR reaction were reported in the literature on Fe-zeolite and other catalysts [1, 3, 5, 6, 14, 25, 34, 36]. There are two notable trends. First, the amount of NO_2 consumed exceeds the amount of NO consumed up to about 300 °C. Since the stoichiometry of the fast SCR reaction (R2) involves an equimolar consumption of NO and NO_2, this means that NO_2 is consumed by another reaction. Second, there is a lack of closure of the overall N-balance; i.e., not all of the N atoms fed are accounted for in the product. These trends are related. The likely culprit is the ammonium nitrate (AN) formation by reaction (R6). AN deposits as a solid onto the surface and cannot be detected in the gas phase by FTIR but can be detected by the FTIR postmortem [5], obviously not as straightforward as in situ gas phase FTIR [3, 5, 6, 27, 34, 36]. For the NO/NOx = 0.5 feed there was ca. 64 and 42 ppm of N missing at the temperatures of 180 and 200 °C, respectively. This implies the formation of 32 and 21 ppm

NH_4NO_3, respectively. The N-balance approached closure with increasing temperature such that by 250 °C there was no net ammonium nitrate formation. Finally, the effect of H_2O was examined for this fast SCR reaction system. Similar to the standard SCR reaction, water was found to have a negligible effect.

At still higher NO_2 feed fractions ($NO/NOx = 0.25$), the NOx reduction activity of Fe/ZSM-5 remains high but shows signs of declining from its peak level (Fig. 11.5c). About 55 % of the NO_2 is converted in the temperature range of 180–200 °C. By 250 °C, the NO_2 conversion increases sharply to >98 %. However, above 350 °C the NO_2 conversion decreases; by 500 °C the NOx conversion is 93 % and the effluent NO concentration increases to 20 ppm. As before, at higher temperatures the NH_3 consumption exceeds the NOx consumption due to NH_3 oxidation (reaction R4). An added feature is the more pronounced production of N_2O at lower temperatures. As in the fast SCR case, the N-balance did not close at lower temperatures (<250 °C), which as described earlier infers the formation of ammonium nitrate. The imbalance of N accounted for an estimated 56 ppm of NH_4NO_3 formed at 180 °C. By 250 °C, the inferred concentration decreased to 9 ppm. At higher temperatures the N-balance closed, suggesting the complete decomposition of ammonium nitrate. The maximum N_2O concentration occurred at 275 °C for this $NO_2/NOx = 0.75$ feed. The decrease in N_2O at higher temperatures is attributed to either its decomposition to N_2 (R15), to its reaction with NH_3 (R16), or to an increase in the rate of NO_2 SCR (R3). Most likely, a combination of these factors contributes to these trends. By 450–500 °C, N_2 was the only N-containing product.

A pure NO_2 feed ($NO_2/NOx = 1$) is a special case in which the standard and fast SCR chemistries are essentially turned off, at least at temperatures below the decomposition of NO_2 (<400 °C). The so-called "NO_2 SCR" reaction (R3) is dominant under these conditions. This reaction to desired product N_2 has NH_3:NO_2 ratio of 1.33, unlike the NH_3:$NOx = 1$ ratio for the standard and fast SCR reactions. The by-products N_2O and NH_4NO_3 are more prevalent compared to their yields at lower NO_2:NH_3 ratios. The integral product distribution data for a dry $NO_2 + NH_3$ feed is shown in Fig. 11.5d. About 60 % NO_2 conversion is achieved at temperatures as low as 180–200 °C. The N-balance did not close under these conditions (ca. 230 ppm was missing in the N-balance at 180 °C), once again indicating the formation of undetected ammonium nitrate. The N-balance inferred that about 115 and 83 ppm of NH_4NO_3 was formed at 180 and 200 °C, respectively. The yields of N_2 and NH_4NO_3 suggest that reaction R6 is the main global reaction occurring under these conditions. A significant amount of N_2O was detected in the temperature range of 225–450 °C. There was a sudden increase in the N_2O concentration from 200 to 250 °C. The maximum amount of N_2O (ca. 250 ppm) occurred at 275 °C. The fate of N_2O at higher temperatures is discussed in more detail later.

The data reveal a significant decrease in the NO_2 concentration between 200 and 250 °C at which point nearly 97 % conversion is achieved. This trend is attributed to an enhanced NO_2 SCR reaction rate. Indeed, the presence of effluent NO clearly indicates the decomposition of NO_2 (reaction R5) while incompletely converted

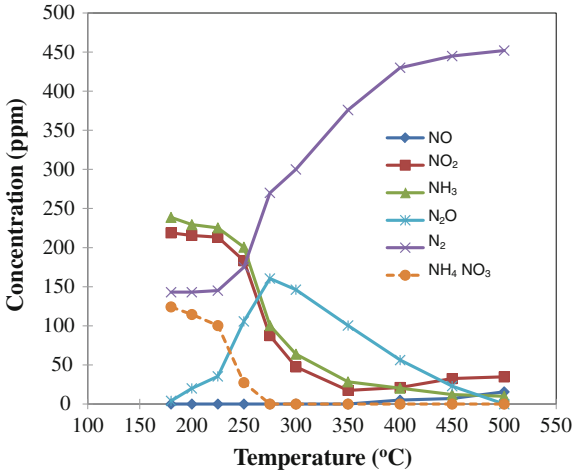

Fig. 11.6 Steady-state product distribution obtained during NO_2 SCR as a function of temperature. Space velocity 57,000 h^{-1}. Total Flow rate = 1,000 sccm. Balance gas: Ar. Feed: 500 ppm NO_2, 500 ppm NH_3, 5 % O_2, and 2 % H_2O

NO_2 suggests depletion of NH_3. Very high NO_2 conversions ($\sim$95 %) are obtained in the temperature range of 250–350 °C but the NO_2 conversion dropped below 90 % at higher temperatures ($T > 400$ °C). Again, this is attributed to the NO_2 decomposition. At still higher temperatures (>350 °C), NH_3 is consumed in somewhat larger amounts compared to NO_2, the signature of ammonia oxidation. Essentially, O_2 competes with NO_2 as an oxidant of NH_3. In contrast, under the fast SCR conditions (equimolar feed NO and NO_2) complete conversion of NOx is obtained at temperatures of 350 °C and higher. The difference in NO_2 and NH_3 consumption also points to the 4:3 NH_3:NO_2 stoichiometry of reaction R3.

The NO_2 SCR reaction system was also carried out in the presence of 2 % H_2O on the Fe-ZSM-5 catalyst. The product distribution (Fig. 11.6) indicates some inhibition of the NO_2 SCR reaction by water. The inhibition is more pronounced in the temperature range of 200–300 °C. A possible reason for this result is that water blocks active sites required for NO_2 SCR. It is also noted that the amount of N_2O, probably generated by the decomposition of NH_4NO_3, decreases in the presence of water. This may suggest that NH_4NO_3 decomposes to NH_3 and HNO_3 (reverse reaction or R10 instead of (R13)) in the presence of H_2O [34].

The experiments with feeds containing NO_2 lead to the generation of N_2O as an important by-product, especially when the feed contains more NO_2 than NO. A negligible amount (<20 ppm) of N_2O is obtained up to NO_2/NOx = 0.5; i.e., standard and fast SCR. For higher NO_2/NOx feed ratios (>0.5), the N_2O yield is prominent for a narrow range of temperatures, as shown in Figs. 11.5d and 11.6 for the NO_2-only feed without and with H_2O, respectively. The increase in N_2O with temperature parallels a decrease in the unaccounted-for N, suggesting that N_2O is formed via NH_4NO_3 decomposition (reaction R3). The formation of N_2O is balanced by its consumption, leading to a maximum in the N_2O yield. For example, for NO_2/NOx feed ratios exceeding 0.75, a maximum N_2O is obtained at

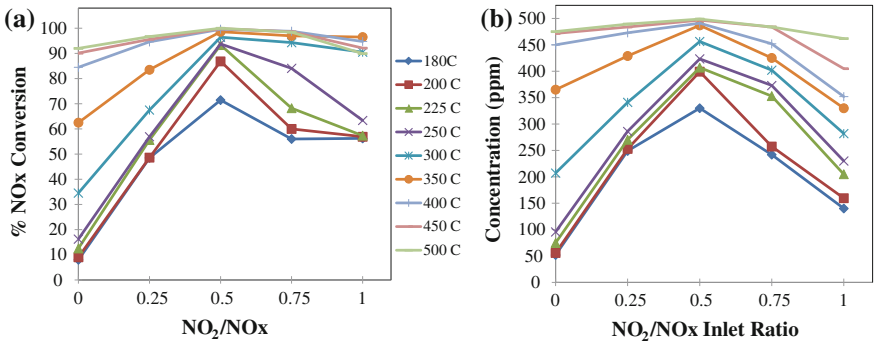

Fig. 11.7 **a** Effect of NO_2/NOx feed ratios and catalyst temperature on the NOx conversion on FeZ-18 catalyst. Space velocity 57,000 h^{-1}. Total Flow rate = 1,000 sccm. Balance gas: Ar. Feed: 500 ppm total NOx, 500 ppm NH_3, 5 % O_2, and 2 % H_2O. **b** Effect of NO_2/NOx feed ratio on N_2 selectivity

about 275 °C. The sharp decrease in N_2O yield with temperature is attributed to two factors:

- The rates of the N_2 selective reactions, i.e., NO_2 SCR, fast SCR, and standard SCR, increase with temperature, and as a result the side reactions responsible for N_2O production decrease.
- The N_2O itself decomposes to N_2 by reaction R15 and hence its effluent concentration decreases at higher temperatures.

The second reason appears more likely. Devadas et al. [34] observed that N_2O decomposes to N_2 and O_2 starting at 350 °C. Our results show that there was no N_2O in the outlet at temperatures above 450 °C. Another possibility for N_2O consumption is reaction with NH_3 (reaction R16). Devadas et al. found that the presence of NH_3 increased the rate of N_2O decomposition. More recently, Colombo et al. [57] reported on data and kinetic modeling for N_2O decomposition and N_2O reduction by NH_3 on Fe-zeolites. In our experiments, we obtained very high NOx conversions (>90 %) for dry feeds and temperatures $\geq$250 °C. NH_3 consumption was nearly 100 % for these temperatures and hence it was difficult to determine how much NH_3 was involved in the reduction of N_2O (R16) and how much NH_3 was oxidized to N_2 (reaction R4). Similar trends for N_2O production on Fe-zeolite and other catalysts were reported in the literature [2, 25, 34, 36].

It is clear that the NO_2/NOx ratio is a critical parameter affecting SCR catalyst performance. The ratio has important effects on both the overall NOx conversion and the product distribution. The effects of NO_2/NOx ratio and temperature on the overall NOx conversion and N_2 yield (concentration) are shown in Fig. 11.7a and b respectively, for a wet feed (2 % H_2O). The conversion data (Fig. 11.7a) show a significant enhancement effect of NO_2 on the deNOx efficiency of the Fe-ZSM-5 catalyst at lower temperatures. At low temperature (180 °C), negligible NOx reduction (<15 %) occurs for the standard SCR reaction. Introduction of 125 ppm

NO_2 increased this value to 50 % while for an equimolar feed the conversion increased to 74 %. This enhancement is attributed to the fast SCR chemistry for which NO_2 is the limiting reactant. As we discuss below, the standard SCR reaction may require the formation of NO_2 to produce N_2. Thus, feeding NO_2 removes this limitation. However, a further increase in NO_2 ($NO_2/NO > 1$) leads to a decrease in the NOx conversion to about 55 % for the pure NO_2 feed. Similar trends were observed for 200 °C. As mentioned earlier, water has a negligible effect on NOx reduction up to the NO_2/NOx feed ratio of 0.5. But for NO_2/NOx feed ratios exceeding 0.5, some inhibition on the NOx reduction was observed in the temperature range of 200–300 °C. The optimum NO_2/NOx ratio for maximum NOx conversion is 0.5 (fast SCR reaction) for the wet feeds, in line with previous literature studies [34, 36].

Along with deNOx efficiency, it is important to achieve a maximum yield and/or selectivity of desired product N_2. The effluent N_2 concentrations indicate that the equimolar feed ($NO_2/NOx = 0.5$) is optimal in terms of N_2 selectivity over the entire temperature range for both the dry and wet feeds (e.g. Figs. 11.5, 11.7b). Unlike the NOx conversion, the N_2 production is a monotonic function of temperature for a fixed NO_2/NOx ratio. This feature suggests the by-product pathways emerge for nonequimolar feeds. Taken together, Fig. 11.7a (NOx conversion) and b (N_2 yield) show that the equimolar NO/NO_2 feed achieves both a high conversion and N_2 selectivity. As NO_2/NOx is decreased below 0.5, the conversion decreases because less NO_2 is available to react with NH_3 and NO via the fast chemistry. As a result, the slower standard SCR chemistry takes over and the conversion declines. For $NO_2/NOx > 0.5$, the emergence of both ammonium nitrate and NO_2 decomposition impact the overall NOx conversion. For temperatures less than 250 °C, the ammonium nitrate is not completely decomposed and inhibits the NOx reduction. For higher temperatures ($\geq$350 °C) some NO_2 decomposition occurs along with 3:4 NO_2:NH_3 stoichiometry of NO_2 SCR, leading to a reduction in the NOx conversion. Ammonia oxidation also emerges at these temperatures. Thus, for temperatures of 350 °C and higher, the highest deNOx conversion was observed for the feed ratio of NO_2/NOx of 0.5; i.e., fast SCR reaction. The fast and standard SCR reactions are clearly beneficial for N_2 formation whereas the pathways to and through ammonium nitrate leads to non-negligible amounts of N_2O. Considering all these factors, a NO_2/NOx ratio of 0.5 proves to be the ideal ratio that achieves maximum NOx removal efficiency and highest product selectivity toward N_2. Similar steady-state results were reported in the literature [12, 34, 36, 58].

11.3 Kinetics and Mechanistic Considerations

The catalytic reaction system containing NO, NO_2, NH_3, O_2, and H_2O on Fe-exchanged zeolites is quite complex as it involves multiple reaction pathways to several products (N_2, N_2O, NH_4NO_3), on catalysts with multiple adsorption sites (Bronsted acid sites, metal-exchanged sites), complicated by rate inhibition

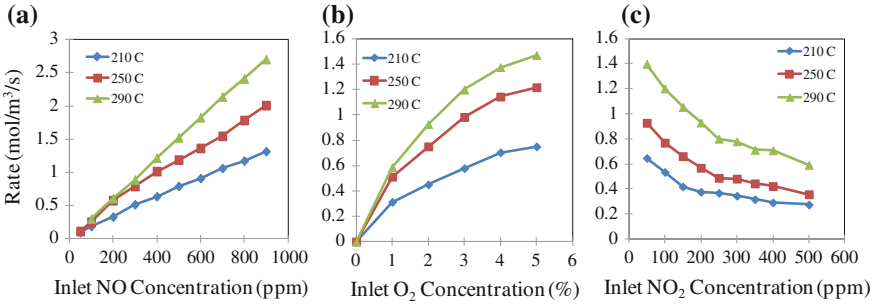

Fig. 11.8 Dependence of differential rate on NO, O_2, and NO_2 during NO oxidation on Fe-ZSM-5. (Adapted from Metkar et al. [56] and used with permission.)

(by NH_3 and NH_4NO_3) and solid deposits (NH_4NO_3) at low temperature, and diffusion limitations (intracrystalline, washcoat) at higher temperatures. In this section we present some of the key kinetics findings, and highlight the current understanding about mechanistic-based kinetics. We will first consider the standard SCR reaction and then proceed to systems containing NO_2 in the feed.

11.3.1 NO Oxidation

Several studies have argued that the oxidation of NO to NO_2, either as a product species in the gas phase or an intermediate adsorbed on the surface, are plausible rate-determining steps for the standard SCR reaction on Fe-exchanged zeolites. If this is the case, then an important first step toward developing a mechanistic-based kinetic model for standard SCR is to establish one for NO oxidation. Metkar et al. [59]. measured the activation energy and reaction orders for NO oxidation on Fe-ZSM-5 (Fig. 11.8). The rate data, which were obtained under differential conditions (fractional conversion, $X_{NO} < 0.15$) at three different temperatures and in the absence of H_2O, revealed apparent reaction orders of 1, 0.5, and −0.3 with respect to NO, O_2, and NO_2, respectively. The inhibition by NO_2 of the forward NO oxidation is not a result of the reversible NO_2 decomposition because that reaction was shown to be negligible at these temperatures. The activation energy was determined to be 39 kJ/mole for the kinetics measurements below 300 °C. The investigators ruled out the existence of washcoat or external transport limitations in this temperature range. In another study, Metkar et al. [42]. showed that the rate of NO oxidation in the absence of H_2O is very close to that of the standard SCR reaction. Figure 11.9 shows the near overlap of the differential rates of NO oxidation and standard SCR at 290–300 °C. The divergence of the two rates at lower temperature is explained by NH_3 inhibition of the SCR reaction, as we elaborate on later. The same study reported that apparent activation energies for the two reactions are quite similar; 39 kJ/mole for NO oxidation and 42 kJ/mole

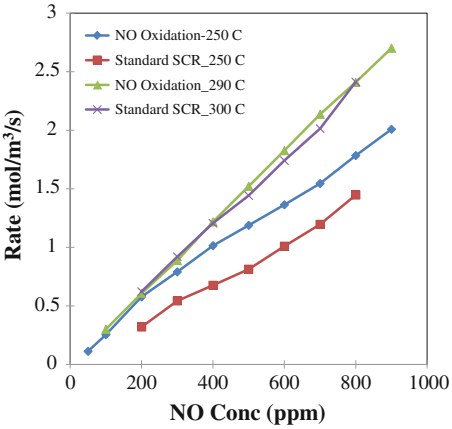

Fig. 11.9 Comparison of differential rates of NO oxidation and standard SCR reaction at two different temperatures. (Used with permission [42] and used with permission.)

for standard SCR. The investigators concluded that the experimental evidence was sufficiently compelling that at the very least the formation of surface-bound NO_2 or related species is the rate-limiting step for standard SCR reaction chemistry.

To this end, it is instructive to compare and contrast two models that have been communicated recently for NO oxidation. The first model is one developed by Harold, Balakotaiah and coworkers and is based on a Langmuir–Hinshelwood framework; it is referred to as the "LH" model. The second model, developed by Tronconi, Nova and coworkers, is based on a redox framework and is referred to as the "Redox" model.

The LH Model comprises the following steps for NO oxidation on Fe-ZSM-5:

$$\text{S1: } O_2 + S_1 \longleftrightarrow O_2 - S_1$$
$$\text{S2: } O_2 - S_1 + S_1 \longleftrightarrow 2O - S_1$$
$$\text{S3: } NO + O - S_1 \longleftrightarrow NO_2 - S_1$$
$$\text{S4: } NO_2 + S_1 \longleftrightarrow NO_2 - S_1$$
$$\text{S5: } 2NO_2 - S_1 \longleftrightarrow NO_3 - S_1 + NO + S_1$$
$$\text{S6: } NO_2 - S_1 + O - S_1 \longleftrightarrow NO_3 - S_1 + S_1$$
$$\text{S5}': 3NO_2 - S_1 + O - \ S_1 \longleftrightarrow \ 2NO_3 - S_1 + NO + 2\ S_1 (\text{sum of S5 and S6})$$

where S_1 denotes an Fe exchange site on the zeolite (Fe-), and therefore O–S_1, NO_2–S_1, and NO_3–S_1 denote an oxygen adatom, adsorbed NO_2 (or nitrite precursor), and nitrate, respectively. The existence of these species is supported by IR measurements and other data, although the situation is potentially more complicated than the listed steps. For example, in an earlier study on protonated pentasil zeolites, Eng and Bartholomew [60] showed in situ IR data confirming the presence of a NO_2−type intermediate on the surface. Rivallan et al. [61] provided "indirect and convincing evidence" for the presence of adsorbed oxygen. Fedeyko et al. [62] provided IR spectroscopic evidence for nitrite/nitrate and nitro groups on Fe-exchanged zeolites and showed that the nitro group is the more reactive of the two. Iwasaki and Shinjoh [63] described a mechanism for nitrate formation that

involves a bi-nuclear site in which NO_2 couples with O positioned between adjacent Fe atoms. Their model considers NO_2 an important surface species. Sachtler et al. [64] proposed that the dimer species N_2O_4, produced via reaction R7, disproportionates on the catalyst surface, yielding NO^+ and NO_3^-. A variant on this mechanism is the production of N_2O_3 through the equilibrium reaction of NO and NO_2 [65]. Subsequently, N_2O_3 disproportionates into NO^+ and NO_2^-, both of which are thought to be reactive NOx surface species upon the addition of NH_3. Given these observations, additional steps and surface species may be warranted in the above six-step LH model.

Now, assuming the reaction between gas phase NO and adsorbed oxygen forming surface-bound NO_2 (S3) is the rate-determining step and all other steps are at equilibrium (including step S5′, the sum of S5 and S6), the following rate expression is derived:

$$R_{\mathrm{NO_{oxi}}} = k_{f3}\sqrt{K_1K_2}\left(X_{\mathrm{NO},s}\sqrt{X_{\mathrm{O_2},s}} - \frac{X_{\mathrm{NO_2},s}}{K_{\mathrm{eq}}}\right)\theta_v \tag{11.1}$$

which, upon solving for θ_v, gives the following rate expression:

$$R_{\mathrm{NO_{oxi}}} = \frac{k_{f3}\sqrt{K_1K_2}\left(X_{\mathrm{NO},s}\sqrt{X_{\mathrm{O_2},s}} - \frac{X_{\mathrm{NO_2},s}}{K_{eq}}\right)}{1 + K_1X_{\mathrm{O_2},s} + \sqrt{K_1K_2X_{\mathrm{O_2},s}} + K_4X_{\mathrm{NO_2},s} + \sqrt{\frac{K_5K_4^3X_{\mathrm{NO_2},s}^3\sqrt{K_1K_2X_{\mathrm{O_2},s}}}{X_{\mathrm{NO},s}}}} \tag{11.2}$$

This complex expression predicts the correct reaction orders and trends in NO oxidation data over a wide range of conditions, such as inhibition by adsorbed NO_2. It is interesting to note that the tuned model predicts that the coverage of the nitrates (NO_3–S_1) is only important at lower temperature and that the four-step model is adequate for predicting steady-state kinetics. Indeed, Yeom et al. [49] argued that nitrites are more reactive than nitrates during SCR to the extent that ammonium nitrate effectively "traps" a NOx molecule as a less reactive species. These points lead to the following simplified rate expression, stressing again that this result is valid when H_2O is absent:

$$R_{\mathrm{NO_{oxi}}} = \frac{k_{f3}\sqrt{K_1K_2}}{1 + K_1X_{\mathrm{O_2},s} + \sqrt{K_1K_2X_{\mathrm{O_2},s}} + K_4X_{\mathrm{NO_2},s}}\left(X_{\mathrm{NO},s}\sqrt{X_{\mathrm{O_2},s}} - \frac{X_{\mathrm{NO_2},s}}{K_{\mathrm{eq}}}\right) \tag{11.3}$$

The situation is more realistic but more complex in the presence of H_2O. Ahrens et al. [66]. pointed out that the formation of nitrates is suppressed through the generation of nitric and nitrous acids. They reported that gas phase NO_2 is effectively removed due to the presence of the acids on the surface at near-ambient conditions. They and others have referred to the well-known chemistry when NO_2 is contacted with H_2O and leads to a mixture of nitrous and nitric acids, which occurs in the upper atmosphere [66, 67]. Some of the more important steps are as follows:

$$\text{S7: } H_2O + S_1 \longleftrightarrow H_2O - S_1$$

$$\text{S8: } 2NO_2 - S_1 + H_2O - S_1 \longleftrightarrow HONO - S_1 + HNO_3 - S_1 + S_1$$

$$\text{S9: } HNO_3 - S_1 + NO + S_1 \longleftrightarrow HONO - S_1 + NO_2 - S_1$$

$$\text{S10: } NO + NO_2 - S_1 + H_2O - S_1 \longleftrightarrow HONO - S_1 + NO_2 - S_1$$

Note that these steps have been written as surface-catalyzed reactions; Ahrens et al. [66] pointed out these steps may also occur in the gas phase. Ross and DeVore [68] showed that HNO_3 desorbs from boehmite at temperatures up to ca. 180 °C. In essence, the additional steps involving water direct the pathways toward a mixture of acids and away from surface nitrites/nitrates. Keeping with the same RDS assumption (step S3), the following rate expression is obtained for θ_v:

$$\theta_v = \frac{1}{1 + K_1 X_{O_2,s} + \sqrt{K_1 K_2 X_{O_2,s}} + K_4 X_{NO_2,s} + K_7 X_{H_2O,s} + \sqrt{K_4 K_{10} K_7 X_{NO_2,s} X_{NO,s} X_{H_2O,s}} + \frac{K_3^2 K_7 K_8 X_{NO_2,s} \sqrt{X_{H_2O,s}}}{\sqrt{K_4 K_7 K_{10} X_{NO_2,s} X_{NO,s}}}} \tag{11.4}$$

Upon the substitution of Eq. (11.4) into (11.1), the resulting rate expression shows the contributions of three new species, H_2O(ad), HONO(ad), and HNO_3(ad), in the denominator. A simplification of the rate expression is possible if it is assumed that the reduction of nitric acid by NO (S9) is fast; this gives:

$$\text{S9}': NO_2 - S_1 + NO + H_2O - S_1 \longleftrightarrow 2HONO - S_1$$

This combined step shows that adsorbed NO_2, a surface nitrite precursor, reacts to give nitrous acid, a key reactive surface species. As we will show later, nitrous acid is an important surface species linking the NO oxidation to standard SCR. Finally, the above rate expression can be further simplified if O–S_1, NO_2–S_1, and H_2O–S_1 are considered the dominant adsorbed species:

$$\theta_v = \frac{1}{1 + \sqrt{K_2 P_{O_2}} + K_3 P_{NO_2} + K_w P_{H_2O}} \tag{11.5}$$

The resulting rate expression predicts the correct trends for NO oxidation in the presence of water such as reaction orders, inhibition, etc.

Recent work by Tronconi and coworkers [54] advocates the Redox model for Fe-based zeolites during NO oxidation in the presence of H_2O. This model builds on mechanism proposals by Kefirov et al. [69], Panov et al. [70], Sun et al. [71], Delahay et al. [41], and Daturi et al. [66]. The mechanistic sequence involves the following steps:

$$\text{S11: } NO + Fe^{3+} - OH \longleftrightarrow Fe^{2+} + HONO$$

$$\text{S12: } HONO + Fe^{3+} - OH \longleftrightarrow Fe^{3+} - ONO + H_2O$$

$$\text{S13: } Fe^{3+} - ONO \longleftrightarrow Fe^{2+} + NO_2$$

$$\text{S14: } 2Fe^{2+} + {}^1/_2O_2 + H_2O \longleftrightarrow 2Fe^{3+} - OH$$

$$\text{S15: } Fe^{3+} - ONO + NO_2 \longleftrightarrow Fe^{3+} - NO_3 + NO$$

The sum of S11–S14 yields the overall NO oxidation reaction (R5). The proposed mechanism involves the oxidation of NO by ferric hydroxide (Fe^{3+}–OH), producing HONO. The production of the Fe nitrite surface species (Fe^{3+}–ONO) subsequently occurs by the reaction of nitrous acid with additional Fe^{3+}–OH. The latter species has been shown to be thermally stable under UHV conditions at temperatures up to ca. 400 °C [70]. Decomposition of the nitrite results in reduction to Fe^{2+} and yields NO_2. Reoxidation of Fe^{2+} occurs with molecular oxygen in S14. The proposed mechanism considers that the decomposition step S13 is the rate-determining step, so steps S11, S12, and S14 are equilibrated and the concentration of nitrous acid and other species is determined by the equilibrium of steps S11 and S12. In essence, the Redox model requires the formation of nitrite for NO_2 to be generated.

The Redox model helps to explain the inhibiting effect of H_2O during NO oxidation. Specifically, an increase in the H_2O concentration decreases the net formation of nitrites and nitrates because of an unfavorable equilibrium of step S12. This supports the observation by Tronconi et al. of negligible DRIFTS evidence for nitrite and nitrate species on Fe-zeolites during NO oxidation in the presence of H_2O [54]. Kamasamudram et al. [11]. compared the low temperature (200 °C) NOx storage during NO oxidation under dry and wet conditions. Appreciable NO_2 evolved from the dry catalyst while the amount evolved from the wet catalyst was negligible. These observations may suggest that the water inhibits the formation of Fe nitrites and nitrates, consistent with the Redox mechanism. The Redox model predicts NO_2 inhibition through the generation of nitrates via reaction step S15. Moreover, the reversible nature of the RDS means that the net rate of NO oxidation is lessened at higher NO_2 concentrations. In addition, NO oxidation is inhibited by NO_2 which suggests that NOx storage is not necessary for site blockage.

A rate expression can be derived if one assumes that HONO, H_2O, and NO_2 as gas phase species, if step S13 is assumed the RDS, and the rest of the steps are therefore at equilibrium. A rate expression comprising steps S11–S15 gives

$$R_{\text{oxi}} = \frac{k_{12}\, C_s \left[K_{10}K_{11}K_{13}p_{\text{NO}}p_{\text{O}_2}^{1/2} - \frac{p_{\text{NO}_2}}{K_{12}}\right]}{1 + \left(K_{13}\, p_{\text{H}_2\text{O}}p_{\text{O}_2}^{1/2}\right)^{1/2} + K_{10}K_{11}K_{13}p_{\text{O}_2}^{1/2}\left(p_{\text{NO}} + K_{14}p_{\text{NO}_2}\right)} \tag{11.6}$$

where C_s is the total site concentration. The expression predicts that the rate dependence on NO is between 0 and 1, on O_2 is between 0 and 0.5, and on NO_2 is between 0 and −1. The expression also predicts inhibition by water.

Several discriminating "Effects" should be considered in assessing the viability of the two competing mechanistic models. These effects include

(I) inhibition of the overall rate of oxidation by water;
(II) removal of Fe nitrites/nitrates by water; and
(III) inhibiting effect of the product NO_2 on the overall rate.

Both models capture Effect (I), the Redox model appears more consistent with Effect (II), while both models predict the NO_2 inhibition Effect (III), albeit in

different ways. Some elaboration on these points is instructive. Both models capture the inhibiting effect of water but the Redox model does so via reaction equilibrium-limited nitrite and NO_2 generation; i.e., nitrite formation is required for NO_2 production. In contrast, the LH model predicts the inhibition through the competitive adsorption of water and of acids generated from the reaction between water and NO_2. Regarding Effect (III), the Redox model considers that NO_2 inhibition is a result of the reversibility of the nitrite decomposition and the generation of surface nitrates. These differences in the models bring to the forefront the question as to whether NO_2, HONO, HNO_3, and even H_2O are, in fact, surface species. That is, disproportionation of NO_2 by water given by S8 is a well-known acid-catalyzed reaction [72]. Whether the acid products HONO and HNO_3 reside on the surface as physisorbed or chemisorbed species is an open question. That said, as described earlier, there is experimental evidence for the existence of adsorbed NO_2 or related species. Such species would be likely to inhibit the oxidation. A variant on the LH model may lead to HONO formation through reaction between NO and surface hydroxyl groups, as in step S11 in the Redox model. Sachtler et al. [49] suggested the formation of a NO^+ active species through the disproportionation of N_2O_3:

$$\text{S16:}\quad N_2O_3 \longleftrightarrow NO^+ - S_1 + NO_3^- - S_1$$

N_2O_3 is present in an equilibrium mixture of NO, O_2, and NO_2 [65]. However, this pathway requires formation of gas phase NO_2 to account for the existence of N_2O_3. Once formed, the NO^+ and surface hydroxyl may react to give surface nitrite, the precursor of nitrous acid

$$\text{S17:}\quad NO^+ - S_1 + S_1 - O^- \longleftrightarrow ONO - S_1 + S_1$$

On the other hand, the direct reaction of gas phase NO with S_1–OH, i.e.,

$$\text{S18:}\quad NO + S_1 - OH \longleftrightarrow HONO - S_1$$

has the appeal of not requiring the formation of NO_2, as would the N_2O_3 decomposition route (S16 and S17) require. Such an Eley-Rideal type step is consistent with the fact that NO negligibly adsorbs. The Redox model as well does not require NO adsorption (S11 and S12).

Final mention should be made of a third mechanism that may be operative that borrows from a known process during Pt-catalyzed NO oxidation: NO_2 generated during NO oxidation leads to the formation of an inactive metal oxide unaffected by water but removed through reaction with NH_3 [55, 73]. During exposure of NO_2, Pt slowly loses its activity over the course of several hours. The activity can be restored upon exposure to a reductant. Were a process similar to this to occur on Fe, then the inhibition could be explained. But Pt is less prone to oxidation while Fe readily forms oxides that are easily reduced for sufficiently high Fe loadings. Clearly, additional work is needed to shed light on the working mechanism that is consistent with steady-state and transient kinetics details and in situ surface species measurements.

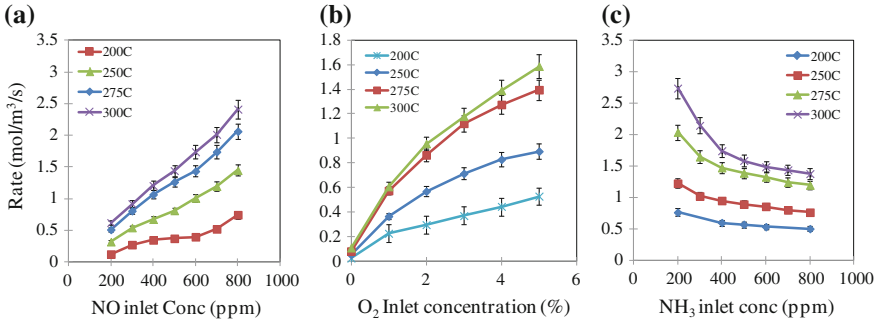

Fig. 11.10 Dependence of differential rate on NO, O_2, and NO_2 during standard SCR on Fe-ZSM-5. (Adapted from Metkar et al. [42] and used with permission.)

11.3.2 Standard SCR Reaction

The addition of NH_3 to the NO + O_2 + H_2O mixture comprises the standard SCR reaction (reaction R1). In this section we discuss possible mechanisms and associated kinetics of this reaction, building on the LH and Redox models for NO oxidation. The activation energy and reaction orders were reported by Metkar et al. [42] for the same catalyst that was studied for NO oxidation. Figure 11.10 shows data indicating orders of 1, 0.5, and −0.3 for NO, O_2, and NH_3, respectively. The corresponding activation energy was determined to be 42 kJ/mole. These data were collected under conditions in which the conversion was less than 15 % and the mass transport limitations were not important. Similar reaction order values were reported by Brandenberger et al. [74] in their detailed kinetics study. Devadas et al. [34] also reported a similar activation energy of 39 kJ/mole. The 39–42 kJ/mole activation energy values compare favorably with the value of 36 kJ/mole reported by Brandenberger et al. [74] who suggested that monomeric Fe species are responsible for a large fraction of the standard SCR at temperatures below 300 °C. They showed that at higher temperatures the reaction occurs on Fe dimers and clusters having a much higher activation energy of 77 kJ/mole. These findings are consistent with the earlier study of Schwidder et al. [21] who proposed that standard (and fast) SCR reactions occur on isolated and oligomeric Fe sites.

A viable rate model derived from a mechanism should be able to predict these measured kinetic parameter values. Unlike NO oxidation, the standard SCR on Fe-exchanged zeolites is not appreciably inhibited by water. Metkar et al. [42] proposed that the inhibition of the NO oxidation is mitigated by the reactive removal of the responsible inhibiting species. This mechanistic picture is supported by earlier work on Fe-zeolites. A fundamental study was carried out by Sun et al. [22] for SCR on Fe/MFI catalyst using isotopically labeled nitric oxide, ^{15}NO. Their data showed that the preferred route to molecular nitrogen involve N atoms from NH_3 and ^{15}NO, giving the mixed product (^{15}NN). On the other hand, undesired oxidation of NH_3 led to the unlabeled product (N_2). From these data,

Sachtler and coworkers suggested that NH_3 "…intercepts this oxidation state of N^{3+} and reduces it to N_2." They argued that an adsorbed intermediate species with oxidation state less than that of NO_2 (N^{4+}) or NO_3^- (N^{5+}) reacted with adsorbed NH_3, forming NH_4NO_2, which then rapidly decomposed to N_2. This may indeed suggest that the above-mentioned step S16, involving N_2O_3 disproportionation to NO^+ and NO_2^-, may supply these species, which then react selectively with NH_3.

The resulting LH type model builds on this concept by considering that adsorbed NH_3 reacts with surface NOx species. It is noted that NH_3 adsorption on Fe-zeolite systems is not inhibited by the co-adsorption of water. A simple interpretation of this key observation is that the adsorption of NH_3 and H_2O occur on different sites. NH_3 adsorption on protonated zeolites is known to occur on the Bronsted acid sites, and that has led Tronconi, Nova, and coworkers among others to propose for vanadia-based catalysts the exchange of NH_3 between two types of sites. Applying this concept for Fe-zeolite catalysts gives:

$$\text{S19:}\quad NH_3 + S_2 \longleftrightarrow NH_3 - S_2$$

$$\text{S20:}\quad NH_3 - S_2 + S_1 \longleftrightarrow NH_3 - S_1 + S_2$$

The selective reduction of NO then proceeds though reaction between the adsorbed NH_3 and HONO:

$$\text{S21:}\quad NH_3 - S_1 + HONO - S_1 \longleftrightarrow NH_4NO_2 - S_1 + S_1$$

NH_4NO_2 is known to be unstable above 100 °C [75]:

$$\text{S22:}\quad NH_4NO_2 - S_1 + S_1 \longleftrightarrow N_2 + 2H_2O - S_1$$

As mentioned above, Sun et al. [22] showed that formation and decomposition of ammonium nitrite is a major route to N_2 with one of the N adatoms originating from NH_3 and the other from NO. Thus, the formation (S21) and rapid decomposition (S22) of ammonium nitrite serves to drive the reversible steps S8–S10 to the right, removing the HONO and related surface species responsible for inhibition of NO oxidation in the presence of H_2O. This may helps to explain why the NO oxidation rate in the presence of water (and absence of NH_3) is considerably slower than the standard SCR rate. Only when the reductant NH_3 is added, is the inhibiting surface species removed, which effectively increases the rate of NO oxidation to surface-bound NO_2.

A kinetic rate model based on the LH mechanism leads to the following result:

$$R_{SCR} = k_1' P_{NO} \sqrt{K_2 P_{O_2}}\, \theta_v' \tag{11.7}$$

where we have simplified the expression for θ_v based on the assumption that the rapid removal of HONO and NO_2 surface through reaction with NH_3; i.e.,

$$\theta_v' = \frac{1}{1 + \sqrt{K_2 P_{O_2}} + K_4 K_5 P_{NH_3}} \tag{11.8}$$

The resulting expression has an inhibition term (denominator) that contains only terms associated with O_2 and NH_3. The functional form of the expression predicts the main trends in the kinetic data for the standard SCR reaction system, such as first order w/r NO, half-order w/r O_2 (when neglecting the term containing Po_2 in the denominator), and negative order w/r NH_3. One cautionary point to note is that in assuming the rate is limited by the production of surface-bound NO_2 (or HONO) with subsequent rapid reaction with adsorbed NH_3, the rate is zero order w/r NH_3 in the limit of $P_{NH3} \rightarrow 0$. In this limit step S21 would become rate limiting and the rate would revert to a positive order dependence w/r NH_3.

The corresponding standard SCR model based on the Redox mechanism for NO oxidation is similar in the sense that adsorbed NH_3 reacts with an intermediate such as HONO

$$\text{S23:}\quad \text{HONO} + \text{ZO}{-}\text{NH}_4^+ + \text{S}_1 \rightarrow \text{ZO}{-}\text{H}^+ + \text{N}_2 + \ 2\text{H}_2\text{O}$$

where ZO–NH_4^+ is NH_3 adsorbed on a Bronsted acid site. Step S23 is similar to the combination of S21 and S22 of the LH model. One difference is that reoxidation of the iron via step S14 is the proposed rate-determining step of the Redox model for standard SCR, as opposed to the formation of NO_2 in the LH model. Thus, the proposal of Ruggeri et al. [54]. is that NH_3 "intercepts" the HONO intermediate. In fact, this proposal borrows from the study of Sun et al. [22]. who, as discussed earlier, suggested a mechanistic picture in which an adsorbed NH_3 reacts with an surface NOx species whose oxidation state is less than that of NO_2. In the absence of NH_3, Ruggeri et al. [54]. suggest that HONO reacts via step S12, forming Fe nitrite, which decomposes to NO_2.

11.3.3 Ammonia Inhibition

A complicating yet interesting feature of SCR on Fe-based catalysts is inhibition by NH_3. The rate described by Eq. (11.8) is based on the assumption that NH_3 adsorbs onto acid sites and then exchanges with metal sites. Differential kinetics data presented earlier (Fig. 11.10) together with other data from the literature show that the rate declines with increasing concentration of NH_3 [42, 62, 74]. Metkar et al. [42] carried out an experiment in which NH_3 was gradually added to a feed containing NO and O_2 without and with water (Fig. 11.11). The addition of NH_3 led to a decrease in the generated NO_2 in both experiments. A simple interpretation of the decreasing NO_2 trend is that NH_3 reacts with NO and O_2 via the standard SCR reaction. This removes an equivalent amount of NO—because of the 1:1 stoichiometry of standard SCR—that would otherwise be oxidized to NO_2. Since the decrease in NO_2 is disproportionately larger, this indicates that the added NH_3 inhibits the surface oxidation of NO to NO_2, considered the rate-determining step for standard SCR in the LH model. It would therefore appear necessary to account for site blocking in the standard SCR kinetic model.

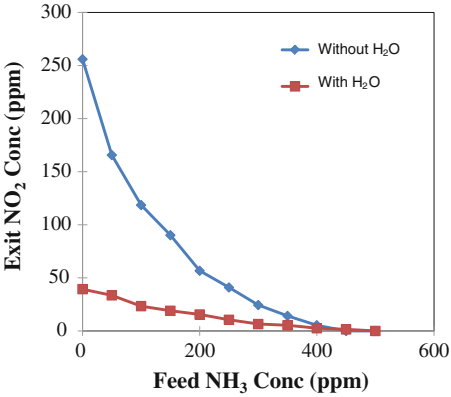

Fig. 11.11 Effluent NO_2 concentration as a function of the concentration of NH_3 fed containing NO and O_2 in the presence (1.5 %) and absence of water. Feed: 500 ppm NO, 5 % O_2, 0 or 1.5 % H_2O. Total flow: 1,000 sccm. Balance gas: Ar. Catalyst Temperature: 350 °C. (Adapted from Metkar et al. [42] and used with permission.)

The standard SCR LH model predicts the inhibition by NH_3 as mentioned earlier in relation to Eq. (11.8). The standard SCR Redox model can also predict NH_3 inhibition through the addition of another step that accounts for NH_3 adsorption on Fe sites. This follows from recent work from the Milano group in which ammonia adsorption can result in hysteresis associated with NH_3 feed transients, among other features.

11.3.4 Selective Catalytic Reaction with NO and NO_2

The chemistry changes dramatically when NO_2 is present in the feed. As presented earlier (cf. Figs. 11.5, 11.7), when $NO_2/NO < 1$ a large enhancement is the NOx conversion is observed with increasing NO_2. On the other hand, NOx reduction inhibition is encountered as NO_2 increases for $NO_2/NO > 1$. The species responsible for the inhibition may be NH_3 and/or NH_4NO_3. As will be shown, the results are much more complex because of the existence of multiple reaction pathways.

We have presented earlier differential kinetics data for the NO oxidation and standard SCR reactions. Here we report on a similar set of experiments involving a feed with different amounts of NO, NO_2, and NH_3. Metkar et al. [42] showed for standard SCR that a space velocity of 285,000 h^{-1} was needed to keep the NO conversion below 15 % in the temperature range of 200–300 °C. In contrast, when the SCR reaction was carried out with an equimolar NO/NO_2 feed, a space velocity of 2×10^6 h^{-1} was needed to ensure differential conversion for temperatures below 245 °C. This high space velocity was achieved by reducing the

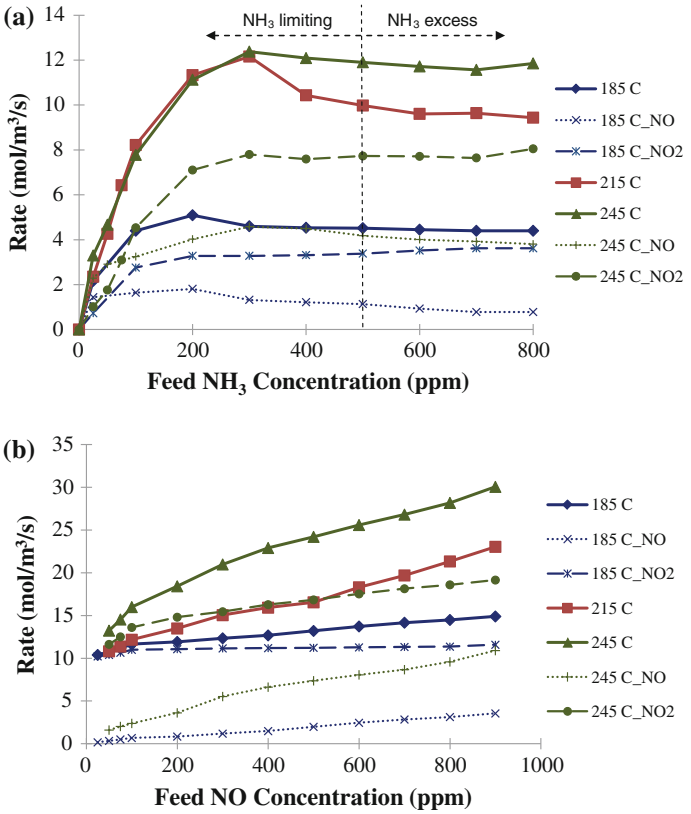

Fig. 11.12 **a** Dependence of differential rate of NO and NO_2 consumption on the feed concentration of NH_3. Space velocity 2×10^6 h^{-1}. Total Flow rate = 1,000 sccm. Balance gas: Ar. Feed: 250 ppm NO, 250 ppm NO_2, 5 % O_2. **b** Dependence of differential rate of NO and NO_2 consumption on the feed concentration of NO. Space velocity 2×10^6 h^{-1}. Total Flow rate = 1,000 sccm. Balance gas: Ar. Feed: 500 ppm NO_2, 1,000 ppm NH_3. **c** Dependence of differential rate of NO and NO_2 consumption on the feed concentration of NO_2. Space velocity 2×10^6 h^{-1}. **d** Dependence of differential rate of NO and NO_2 consumption on the feed concentration of NO_x ($NO = NO_2$). Total Flow rate = 1,000 sccm. Balance gas: Ar. Feed: 500 ppm NO, 1,000 ppm NH_3

size of the catalyst to 4 channels and 5 mm length with the total flow rate maintained at 1,000 sccm. Since the temperature was below 300 °C, the decomposition of NO_2 was negligible. The effluent NO and NO_2 concentrations were used to calculate an average rate normalized by the washcoat volume using 50 μm as the estimated thickness. We refer to the overall NOx consumption rate as R_{NOx}, the NO_2 rate as R_{NO_2}, and the NO rate as R_{NO}. The results from three experiments shown in Fig. 11.12a–d, respectively, report these rates as a function of NO, NO_2, and NH_3 over the 185–245 °C temperature range. Higher temperatures were not considered because differential conversion could not be achieved.

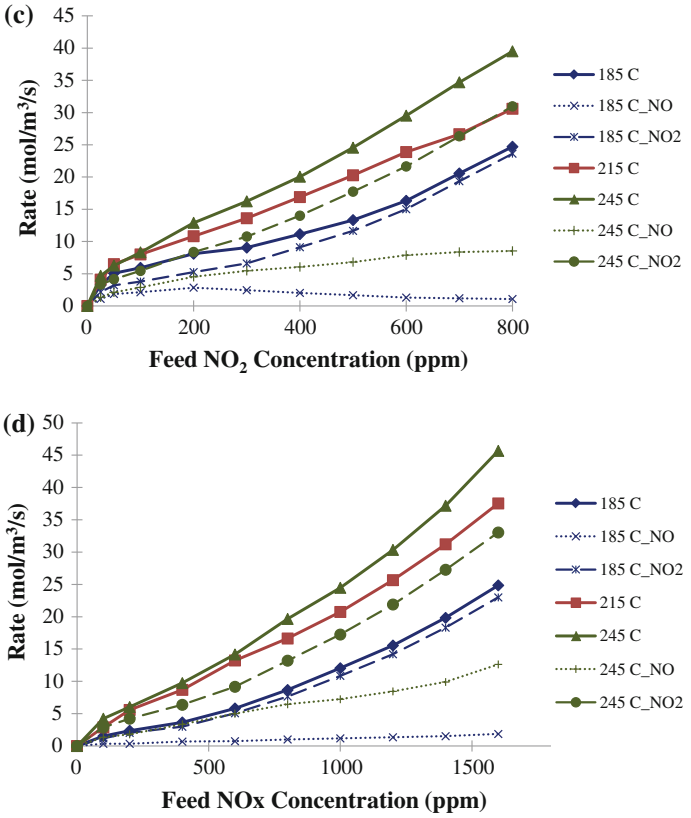

Fig. 11.12 continued

It should be mentioned that washcoat diffusion limitations become more important for the fast SCR reaction. As discussed in more detail later, diffusional limitations emerge at a rather low temperature for fast SCR; ca. 225 °C for an Fe-ZSM5 catalyst having a ca. 24 % mass loading (Metkar et al. [76]). For this reason, diffusional limitations cannot be ruled out for the 245 °C differential rate data.

The data reported in Fig. 11.12a show the dependence on NH_3 concentration with the NO and NO_2 concentrations each fixed at 250 ppm, O_2 fixed at 5 %, and no H_2O in the feed. The total NOx reduction rate for three temperatures and the individual NO and NO_2 consumption rates are shown for the bounding temperatures. The figure reports the individual rates of NO and NO_2 consumption; their sums equal the overall rate, R_{NOx}. Indicated in the figure is the NH_3 concentration at which the fast SCR feed is achieved. To the left of that point the reaction system is deficient in NH_3, while to the right the NH_3 is in excess with respect to the stoichiometry ratio $NO:NO_2:NH_3 = 1:1:2$. For each of the three temperatures R_{NOx} exhibits a slight maximum, with the maximum shifting to higher NH_3 concentration with increasing temperature. To the right of the maximum the total

rate slightly decreases with increasing NH_3 concentration, although the data indicate that the decrease is somewhat more pronounced at the higher temperatures. To the left of the rate maximum, an interesting feature is the coincidence of the 215 and 245 °C R_{NOx} data. At each temperature, the NO_2 consumption rate (R_{NO_2}) exceeded the rate of NO consumption (R_{NO}) except when NH_3 was less than 100 ppm. Below that concentration $R_{NO_2} < R_{NO}$

The trends in the rate data as a function of NH_3 in Fig. 11.12a reveal two notable features. First, the existence of the rate maximum is evidence for inhibition by NH_3, encountered during standard SCR (Fig. 11.10). At higher NH_3 concentration the NH_3 blocks sites for adsorption and reaction. In the case of standard SCR, ammonia blocks the adsorption of oxygen and hence the conversion of NO into NO_2. In the case of fast SCR, ammonia similarly blocks the adsorption of NO_2, a necessary step for the subsequent formation of nitrites/HONO that reacts with NH_3 to form N_2. Second, the inequality of the NO and NO_2 consumption rates suggests that multiple paths to N_2 occur simultaneously. The fast SCR stoichiometry (reaction R2) implies the rates should be equal. But the equimolar NO/NO_2 feed containing 500 ppm NH_3 shows that the NO_2 consumption rate is nearly twice that of NO consumption. This suggests that NO_2 is consumed by an additional route such as reaction R3 ("NO_2 SCR") and/or R6 (AN formation). This trend is consistent with the integral consumption of NO and NO_2; i.e., the fast SCR feed case shown in Fig. 11.5b indicates that NO_2 is consumed more rapidly than NO as a function of temperature. It is interesting to note in Fig. 11.12a that the NH_3 appears to inhibit the rate of NO but not of NO_2 consumption. This subtle feature needs further investigation because it may mean that the adsorption of NO_2 is not inhibited to the same degree as the adsorption of oxygen. When NH_3 is below 100 ppm, the NO consumption rate overtakes that of NO_2. This feature also deserves further consideration.

A similar experiment was carried out for NO and the results are reported in Fig. 11.12b. In this experiment, the dry feed NH_3 and NO_2 concentrations were kept constant at 1,000 and 500 ppm, respectively, while the NO feed concentration was varied from 0 to 900 ppm. O_2 was not fed in order to avoid the occurrence of the standard SCR and NH_3 oxidation by O_2 reactions. The total NOx consumption rate is an increasing function of the NO concentration at all temperatures but steeper at lower concentrations, indicating an apparent NO order less than unity. This is in contrast to an order of unity for the standard SCR reaction (Fig. 11.10). Like the results with NH_3 in Fig. 11.12a, the NO_2 consumption rate exceeds the NO consumption rate. In contrast with the NH_3 experiment, however, at a NO concentration of zero the NO_2 consumption rate is nonzero due to the direct reaction between NO_2 and NH_3 that does not require NO. On the other hand, the NO consumption rate passes through the origin. That the NO consumption rate is nonzero in the absence of O_2 points to reaction of NO with surface nitrates, forming NO_2; i.e., reverse of reaction S5.

Similar studies were repeated by varying the feed NO_2 concentration in the same temperature range (Fig. 11.12c). NO and NH_3 feed concentrations were kept constant at 500 and 1,000 ppm, respectively. Again, no O_2 was present in the feed.

In this experiment all of the rate curves pass through the origin. This shows that NO reaction with NH_3 is negligible in the absence of NO_2 or O_2. The data also show that the apparent reaction order with respect to NO_2 is positive. In fact the shapes of the NO_2 consumption rate curves are sigmoidal, while the NO rate curves exhibit a shallow maximum. These are features should be predicted by any viable kinetic model.

In addition to the experiments shown in Fig. 11.12a–c, we simultaneously increased NO and NO_2 concentrations in the feed while holding the NH_3 concentration fixed. NO and NO_2 were fed in equimolar ratio while keeping the NH_3 constant at 1,000 ppm and the feed gas devoid of O_2. The data in Fig. 11.12d shows that the NOx consumption rate is an increasing function of the equimolar NOx feed. Moreover, a sigmoidal character to the data is apparent. As in the above-described experiments, the NO_2 consumption rate exceeded that of NO. This trend is consistent with earlier results obtained for integral NOx conversion experiments.

Similar experiments were carried out to determine the effect of oxygen concentration on the fast SCR reaction. For these experiments, 500 ppm NO, 500 ppm NO_2, and 1,000 ppm NH_3 were kept constant in the inlet feed and Ar was used as a balance gas with 1,000 sccm as the total flow rate. The inlet O_2 concentration was varied in the range of 0–5 % for temperatures of 185, 220, and 245 °C. The O_2 was found to have no effect on the fast SCR reaction. Hence the apparent reaction order with respect to O_2 can be considered to be zero.

From these rate data the following observations can be made. The NOx consumption rate for the fast SCR reaction has apparent positive orders with respect to both NO and NO_2. However, the complex dependence on NO_2 in particular indicates multiple reaction pathways in the presence of NO. The apparent order for ammonia varies between positive and negative while the apparent reaction order for O_2 is nearly zero. From Fig. 11.12a it is clear that the increasing NH_3 reduces the R_{NO} slightly while having a negligible effect on R_{NO_2}. Grossale et al. [40] described the role of NH_3 inhibition on the fast SCR chemistry at lower temperatures. They concluded that the NH_3 blocking effect is due to the strong interactions between NH_3 and nitrates. That is, fast SCR is inhibited by AN formed through the reaction of NH_3 and surface nitrates. To this end, NO reduction of AN is a plausible rate-determining step. Below we describe an experiment that provides additional evidence for this. Finally, the apparent activation energy for the fast SCR reaction with respect to the rate of NOx conversion at different temperatures was found to be 18 kJ/mol, which is somewhat less than that of standard SCR reaction (ca. 40 kJ/mole). Devadas et al. [34]. reported a value of about 7 kJ/mol for the fast SCR and temperatures up to 350 °C. At this temperature, diffusion limitations cannot be ruled out and thus the value they have obtained may not be valid for the intrinsic kinetic regime. An examination of mass transfer is presented in the next section.

Transient experiments provide additional probes of mechanistic issues not obtainable from steady-state experiments. Studies by Tronconi and coworkers

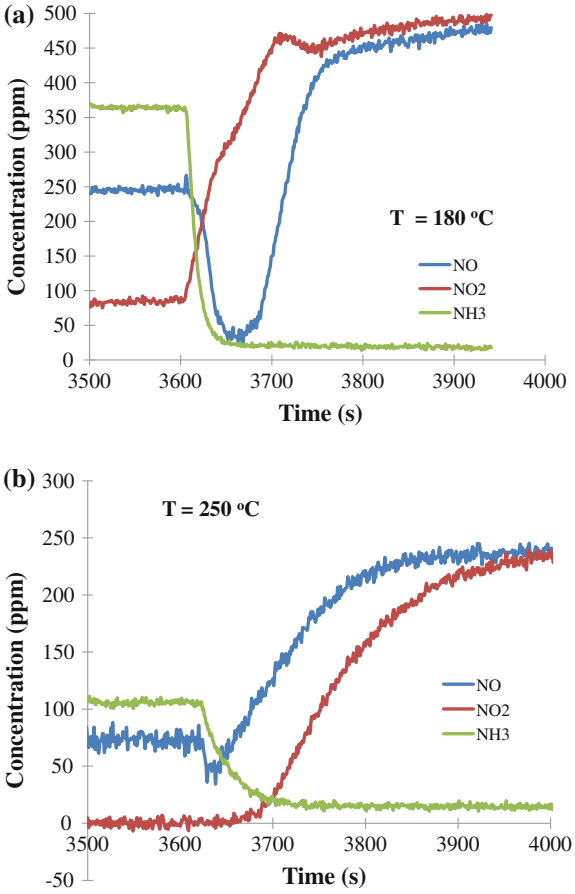

Fig. 11.13 Dependence of species concentrations on time for experiment in which NH_3 was shut off at $t = 3{,}600$ s mark; in **a** the temperature was 180 °C whereas in **b** the temperature was 250 °C

have illustrated this for V-based catalysts [48] and Fe-based catalysts [27]. Here we describe similar experiments carried out at UH. In order to study the ammonia inhibition effect in more detail, we carried out transient experiments in which a mixture containing 500 ppm each of NO and NO_2, and 1,000 ppm NH_3 was fed to the reactor for 1 h and then NH_3 was suddenly switched off. The transient response of the NO and NO_2 concentrations was monitored during this procedure. Figure 11.13a, b shows the results obtained at 180 and 250 °C, respectively. The premise of the experiment was to examine if any ammonia nitrate was present on the catalyst. At 180 °C, immediately after the NH_3 stoppage it was observed that the NO concentration dropped for a while, went through a minimum and then increased; in contrast, the NO_2 and N_2 both increased with the stoppage of NH_3. Thus, NO was apparently being consumed at 180 °C. At 250 °C, the dip in NO concentration was small, while at 300 °C, no dip in the NO concentration was observed. These observations indicated that the dip in NO concentration is due to the reaction of NO with NH_4NO_3 present on the catalyst (reaction R11).

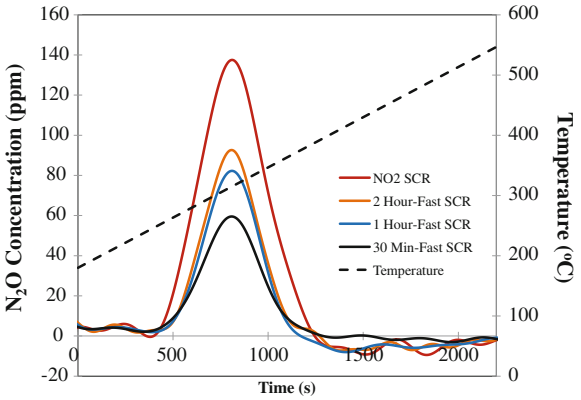

Fig. 11.14 Comparison of N_2O evolved obtained during the temperature programmed desorption (TPD) after catalyst was exposed to four different reaction conditions at 180 °C. A temperature ramp of 10 °C/min was applied evolve the N_2O from the catalyst. The Fast SCR experiments involved a feed mixture containing 500 ppm NO, 500 ppm NO_2, 1,000 ppm NH_3, 5 % O_2 fed to the reactor for durations of 30 min, 1, and 2 h. The NO_2 CR experiments involved a feed mixture of 1,000 ppm NO_2, 1,000 ppm NH_3, and 5 % O_2 for a duration of 2 h

As observed in the steady-state experiments above, the NH_4NO_3 present on the catalyst decreased with time and at 300 °C, there was essentially no NH_4NO_3 present for the fast SCR case.

To examine the effect of NH_4NO_3 formation on the overall conversion, we carried out some TPD experiments after the catalyst was exposed to a feed containing 1,000 ppm of both NH_3 and NOx (NO + NO_2) in the presence of 5 % O_2 for different durations (between 0.5 and 2 h); see Fig. 11.14. The catalyst temperature was maintained constant at 180 °C during this exposure. After the prescribed time had lapsed, all the gases except Ar were switched off for 30 min to remove any physisorbed species, and then a temperature ramp of 10 °C/min was applied. During the temperature ramp, N_2O was evolved, reaching a peak value in the temperature range of 250–300 °C. The amount of N_2O generated, which was calculated by integrating the N_2O peak, provided an estimate of the amount of NH_4NO_3 present on the catalyst; i.e., the AN decomposition product is N_2O. The amount of N_2O evolved was different for each of the feeds. The largest amount evolved was obtained for the 2 h experiment with 1,000 ppm NO_2. This amount exceeded by more than 50 % the amount obtained during the 2 h experiment with the equimolar mixture of NO_2 and NO (0.43 mol). The 1 h long equimolar feed resulted in only slightly less N_2O evolved (0.37 mol), indicating that the catalyst had reached a constant level of AN by 2 h even though the catalyst had capacity for additional NH_4NO_3 accumulation at this temperature (based on the NO_2 + NH_3 exposure). At the very least, these experiments demonstrate that NH_4NO_3 is present on the catalyst surface and that it is the probable inhibiting species in this temperature range. The lesser amount accumulated with the NO=NO_2 feed compared to the NO_2 feed indicated a mitigating role of the NO.

The likely explanation is that NO served to react with (reduce) the NH_4NO_3, freeing up sites and increasing the conversion. Furthermore, the rather slow approach to steady state in these experiments indicated that the reduction of NH_4NO_3 by NO is a likely rate determining under these conditions.

Various mechanistic-based kinetic models that describe the effect of NO_2 have appeared in the literature. Here we attempt to summarize the current understanding of the mechanism and associated kinetics. As before, we consider both the LH and Redox approaches.

Tronconi and coworkers have proposed a fast SCR kinetic mechanistic model that is based on a Redox mechanism [27, 57, 58]. Like the LH SCR model, the Redox SCR model has adsorbed NH_3 reacting with gas phase HONO or surface nitrites, forming NH_4NO_2, which decomposes to N_2 (cf. S22). The nitrites are formed through the reduction of nitrates by NO (step S9). Additional steps would include the formation of NH_4NO_3 and its decomposition to N_2O, among others.

The role of NO_2 during SCR was considered by Grossale et al. [19, 77] in the context of a redox process. For example, they proposed a series of global reactions that would explain the 3:4 NO_2:NH_3 stoichiometry of the NO_2 SCR reaction R3 in the presence of H_2O.

$$\text{R17: } 6NO_2 + 3H_2O \longleftrightarrow 3HNO_3 + 3HONO \qquad \Delta H = -20.6 \times 10^3 \text{J/mol } NO_2$$

$$\text{R18: } 3HONO + 3NH_3 \longleftrightarrow 3N_2 + 6H_2O \qquad \Delta H = -358 \times 10^3 \text{J/mol HONO}$$

$$\text{R19: } 3HNO_3 + 5NH_3 \longleftrightarrow 4N_2 + 9H_2O \qquad \Delta H = -513 \times 10^3 \text{J/mol } HNO_3$$

The investigators coined the term "fast ammonia oxidation" reaction system. The global reactions are similar to the surface reactions contained in the context of the LH fast SCR model. One difference is that in the absence of NO the reduction of surface nitrate does not occur. In related work, the Milano group showed among other things that surface nitrates are preferentially reduced by NO, if available; i.e., fast SCR. In the absence of NO the nitrates are less effectively reduced by NH_3; i.e., NO_2 SCR [27]. The alternative LH model considers that for a feed consisting of NO, NO_2, and NH_3 (in excess O_2 and H_2O) the co-adsorption of NO_2 and NH_3 is followed by a series of steps that lead to the acidic species HONO and HNO_3:

$$\text{S4: } NO_2 + S_1 \longleftrightarrow NO_2 - S_1$$
$$\text{S5:} 2NO_2 - S_1 \longleftrightarrow NO_3 - S_1 + NO + S_1$$
$$\text{S6: } NO_2 - S_1 + O - S_1 \longleftrightarrow NO_3 - S_1 + S_1$$
$$\text{S7: } H_2O + S_1 \longleftrightarrow H_2O - S_1$$
$$\text{S8: } 2NO_2 - S_1 + H_2O - S_1 \longleftrightarrow HONO - S_1 + HNO_3 - S_1 + S_1$$
$$\text{S9: } HNO_3 - S_1 + NO + S_1 \longleftrightarrow HONO - S_1 + NO_2 - S_1$$
$$\text{S10: } NO + NO_2 - S_1 + H_2O - S_1 \longleftrightarrow HONO - S_1 + NO_2 - S_1$$
$$\text{S19: } NH_3 + S_2 \longleftrightarrow NH_3 - S_2$$
$$\text{S20: } NH_3 - S_2 + S_1 \longleftrightarrow NH_3 - S_1 + S_2$$

The LH model, like the Redox model, considers that the reaction of the acids with surface NH_3 leads ultimately to NH_4NO_2 and NH_4NO_3. The nitrite pathway is the selective one to N_2

$$\text{S21: } NH_3 - S_1 + HONO - S_1 \longleftrightarrow NH_4NO_2 - S_1 + S_1$$
$$\text{S22: } NH_4NO_2 - S_1 + S_1 \longleftrightarrow N_2 + 2H_2O - S_1$$

The nitrate pathway can lead to N_2 but also involves a nonselective decomposition pathway to by-product N_2O

$$\text{S24: } NH_3 - S_1 + HNO_3 - S_1 \longleftrightarrow NH_4NO_3 - S_1 + S_1$$
$$\text{S25: } NH_4NO_3 - S_1 \longleftrightarrow N_2O + 2\ H_2O - S_1$$

In addition, the NO reduction of AN, analogous to HNO_3 reduction, is plausible, following the above-described experiments which quantified the net production of AN; i.e.,

$$\text{S26: } NH_4NO_3 - S_1 + NO + S_1 \rightarrow NH_4NO_2 - S_1 + NO_2 - S_1$$

Finally, the "NO_2 SCR" reaction R3 involves a selective pathway to N_2.

The LH model comprising this set of steps can be used to derive a governing rate expression if a single rate-determining step is identified. Which step is the limiting one will depend on the relative quantities of NO and NO_2. In the limit of the feed $NO_2 \rightarrow 0$, the mechanism should resort to the standard SCR reaction which would have to include NO oxidation steps S1, S2, and S3. With increasing NO_2 in the feed, the conversion data clearly shows an enhancing effect of NO_2. The overall chemistry is de-bottlenecked following the argument that the formation of adsorbed NO_2 is the rate-limiting process in the $NO_2 \rightarrow 0$ limit. Then the formation of the two key intermediates, NH_4NO_2 and NH_4NO_3, are the primary, potentially limiting pathways affecting the conversion and product distribution. The rates of interconversion of their precursors, nitrous and nitric acids and/or Fe nitrites and nitrates, are critical. For example, when NO is added systematically to a feed containing NO_2 and NH_3, an increase in the N_2 yield and decrease in the NH_4NO_3 yield results (Fig. 11.15). It has been shown that the addition of NO causes the reduction of nitrates to nitrites [36, 77]. The aforementioned transient tests (Fig. 11.14) underscore this point. Indeed, the fact that the highest rates are obtained with an equimolar mixture is explained by the sum of steps S8 and S9

$$\text{S9}'\ (= \text{S8} + \text{S9}):\ NO_2 - S_1 + NO + H_2O - S_1 \longleftrightarrow 2HONO - S_1$$

That is, the role of NO is to convert nitrates to nitrites, which are rapidly converted to N_2 in the presence of NH_3. This follows from earlier works advocating the Redox model, such as Grossale et al. [27]. The analog of step S9' indeed represents a redox step involving the change in the formal oxidation state of N from +5 (nitrates) to +3 (nitrites). Earlier we showed transient kinetic evidence that the NO reduction of NH_4NO_3 (step S25) may be rate determining at lower temperature. A similar reaction is the NO reduction of nitric acid (S9) or nitrates.

These steps increase the coverage of surface nitrites which rapidly convert to N_2. The differential rate data for temperatures below 250 °C presented earlier show clear evidence for multiple reaction pathways: The differential rate of NO_2 consumption exceeds that of NO at lower temperatures. This points to the formation of NH_4NO_3 and its inhibition of N_2 formation, but also the mitigation of the inhibition by and AN reduction by NO. It can be shown that an overall rate based on the reduction of HNO_3 and/or NH_4NO_3 as the RDS has the functional features to predict the main trends in the experimental data. Further analysis of microkinetic models that include these steps S1–S10 and S19–S26 is needed. Later we describe global kinetic models that predict these data as a first step toward this goal.

In the limit of the feed $NO_2/NOx \rightarrow 1$, the LH mechanism should predict the NO_2 SCR reaction behavior. That the overall stoichiometry to N_2 product is 4:3 NH_3:NO_2 and not 1:1 points to the different chemical pathways. In the absence of gas phase NO, the reduction of HNO_3 or NO_3^- will not occur. This helps to explain why NH_4NO_3 and its decomposition product N_2O are important by-products at low to moderate temperatures. On the other hand, at high temperatures (>400 °C) NO_2 decomposition will occur, yielding adsorbed NO and O. Moreover, adsorbed NH_3 may react with O adatoms forming N_2 and NO as products. In turn, the NO can then serve in the role of reductant, generating $HONO/NO_2$ through reaction with HNO_3/NO_3^-. Detailed kinetics data are needed to build such a mechanistic-based model.

11.4 Reaction and Transport Interactions

An important aspect of catalytic reactor design is understanding, quantifying, and managing mass and heat transport limitations. While heat transport limitations are negligible in NH_3-based SCR due to the low reactant concentrations, mass transport limitations cannot be similarly ruled out. This includes mass transport at three levels: external mass transport from the bulk gas to the catalyst surface, washcoat diffusion within the mesoporous layer containing zeolite crystallites supported by a high surface area binder material such as alumina, and crystallite-scale diffusion within the pores of the zeolite crystallites. In practice, zeolite diffusion is lumped with the intrinsic catalytic processes due in part to the difficulty of separating the two processes. Here we highlight our understanding of the impact of the first two processes on the SCR catalyst performance in a monolith containing a washcoat of Fe-exchanged zeolitic crystallites (Fig. 11.15).

In a recent study, Metkar et al. [78] presented a systematic analysis in which the washcoat loading and monolith length were varied to quantify the extent of diffusion limitations during SCR on an Fe-exchanged monolith catalyst. Figure 11.16 compares the conversions obtained with two Fe-ZSM-5 catalysts having the same total washcoat loadings but different washcoat aspect ratios (thickness, length). Each catalyst was subjected to the same conditions; since this included total flow rate the ratio of the catalyst mass and total flow rate (W/F value) was fixed. This

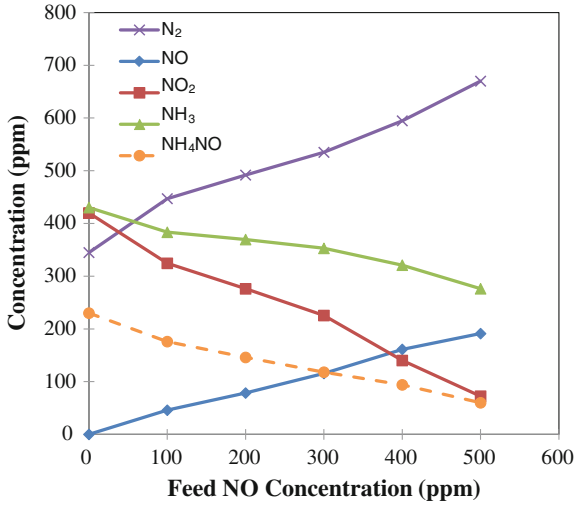

Fig. 11.15 Effect of feed NO concentration on the product distribution during SCR on FeZ-18 catalyst at 185 °C. Space velocity 57,000 h^{-1}. Total Flow rate = 1,000 sccm. Balance gas: Ar. Feed: 1,000 ppm NOx (NO + NO_2), 1,000 ppm NH_3, 5 % O_2, and 2 % H_2O

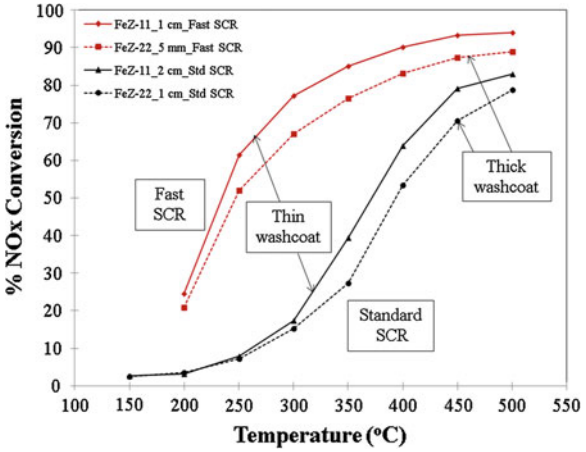

Fig. 11.16 Dependence of steady-state NOx conversion versus temperature for fast and standard SCR on two different catalysts. FeZ-22: 5 mm (fast SCR) and 1 cm (standard SCR); Fe-11: 1 cm (fast SCR) and 2 cm (standard SCR). Feed conditions: 500 ppm NOx, 500 ppm NH_3, 5 % $_{O2,}$ balance Ar; 1,000 sccm (GHSV = 57 K h^{-1}). (Used with permission [78] and used with permission.)

method identifies the emergence of washcoat diffusion limitations as the temperature is increased. In the purely kinetic regime no difference would be encountered because the catalyst is fully utilized. In the case of a very fast reaction external

mass transport limitations emerge at high temperatures. In this latter case only a small fraction of the washcoat would be utilized. The fixed W/F test could be augmented by an experiment in which the residence time is maintained constant to provide additional insight about external mass transfer.

The analysis of Metkar et al. shows that for standard and fast SCR on Fe-exchanged zeolites, the extent of mass transport limitations varies but appears to be important for most practical operating conditions and typical washcoat loadings. The results obtained on different Fe-exchanged zeolite samples clearly show the onset of mass transport limitations above a threshold temperature. That temperature value depends on the SCR feed composition (standard, fast, NO_2 types). A threshold temperature of about 300 °C for standard SCR and 250 °C for fast SCR was estimated. An estimate of the apparent activation energy that was about half the value determined when mass transport limitations were negligible provided further evidence. Metkar et al. [42] reported an apparent activation energy of 24 kJ/mole during differentially operated standard SCR on the same washcoated Fe-ZSM-5 in the temperature range of 350–500 °C. A smaller sample enabled a high space velocity (2×10^6 h^{-1}) to achieve the differential conditions. The 24 kJ/mole was slightly over one-half the value obtained at lower temperatures (42 kJ/mole). The one-half value of the apparent activation energy is a signature of diffusion limitations. Metkar et al. showed how the analysis can also be used to estimate the effective diffusivity through the use of the Weisz-Prater modulus and confirmed by simulations using a 1 + 1 D monolith reactor model. An activation energy as low as 7 kJ/mole was reported by Devadas et al. [23] for fast SCR and may indicate the presence of external mass transport limitations. A study by Nova et al. [79] indicated the presence of transport limitations for Cu-zeolite catalysts. Monoliths having three different cell densities (200, 400 and 600 CPSI) were compared for the same mass loading of washcoat. The study concluded that diffusional limitations were present for the 200 CPSI monolith catalysts and possibly the 400 CPSI sample. On the other hand, a more recent study by Colombo et al. [57] indicated that diffusion limitations are negligible to modest based on a comparison of monolith and crushed monolith powder catalysts. The authors cautioned about the generalization of these findings. Differences in the extent of transport limitations can be attributed to differences in the intrinsic activities of the catalysts, for example. In summary, it is clear that the issue of diffusion limitations is a nontrivial one but deserves attention in the design of SCR reactors.

Indisputable experimental evidence for the existence of diffusional limitations is the data from a study of dual-layer Fe–Cu zeolite catalysts carried out by Metkar et al. [80]. In that study, monoliths were sequentially coated with layers of Cu- and Fe-exchanged zeolite catalyst. The results showed that a monolith comprising a top layer of Fe-ZSM-5 and a bottom layer of Cu-ZSM-5 resulted in an expanded, high NOx conversion temperature window. At sufficiently high temperature the dual layer catalyst conversion approached that of the single layer, Fe-only catalyst, suggesting that only the top Fe layer of the dual component was utilized. That is, washcoat diffusion limitations of the limiting reactant, in this case NH_3, prevented the utilization of the underlying Cu layer. With feeds spanning standard, fast, and

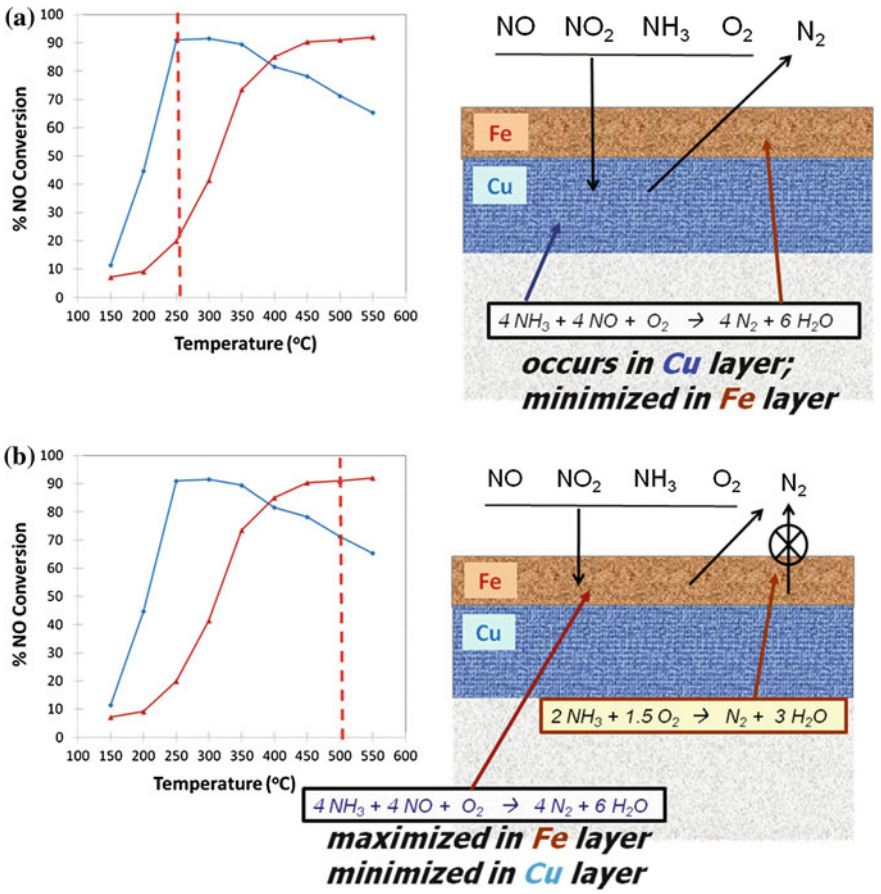

Fig. 11.17 Schematic representation of dual layer Fe/Cu monolith catalyst. (Used with permission [80].)

NO_2 SCR compositions, superior NOx conversion performance was achieved with the layered architecture. The schematic shown in Fig. 11.17 explains the concept while Fig. 11.18 provides typical data for several monolith samples. The catalyst design and operating strategy was to exploit differences in the intrinsic activity and selectivity of the two catalysts through coupled reaction and diffusion. At low temperature the top layer should behave in the limit as simply as a diffusion barrier, whereas at high temperature the top layer should be sufficiently active so as to confine most of the conversion in that layer. This was of definite benefit because at low temperature, the Fe layer was much less active than the underlying Cu layer which was selective for N_2, while at high temperature reaction occurred in the more selective Fe top layer.

To illustrate, the data in Fig. 11.18 shows that a washcoat catalysts containing different fractions of Fe and Cu but a fixed total loading result in quite different

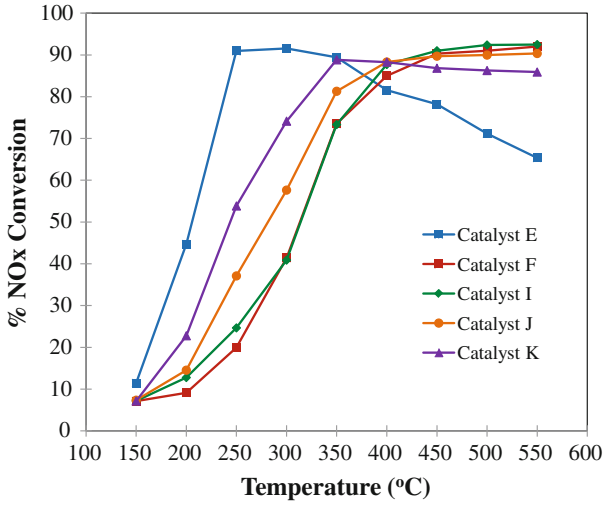

Cat.	Cu-Z Loading (wt %)	Fe-Z Loading (wt %)
E	25	0
F	0	24
I	8	16
J	12	12
K	16	8

Fig. 11.18 Dependence of steady-state NOx conversion versus temperature for several monolith catalysts with compositions shown in table. (Adapted from Metkar et al. [80] and used with permission.)

NOx conversions. The 50:50 Fe:Cu-layered catalyst achieved a NOx conversion that was essentially the arithmetic average of the individual Fe- and Cu-exchanged catalysts. In contrast, the dual layer catalyst with a thin Fe-zeolite (33 % of the total washcoat loading) layer on top of a thicker Cu-zeolite layer (67 %) resulted in a high NOx conversion over a wide temperature range and NO_2/NOx feed ratio values. In the lower temperature range, the conversion approached that of the Cu-zeolite, whereas at higher temperatures the conversion approaches that of the Fe-zeolite.

These dual layer results provide clear evidence of the existence of mass transport limitations. That the conversion for the dual-layer Fe/Cu catalyst (I, J, K) approached that for the Fe (top) layer at sufficiently high temperature indicates that significant transport limitations were present. In fact, the experiment helps to pinpoint the temperature at which the onset of diffusion limitations occurs for an Fe top layer of a prescribed loading (thickness). As the Fe top layer thickness decreases, the temperature at which the dual layer catalyst conversion is within a few percent of the single layer Fe catalyst (sample F) conversion increases. For example, the conversion for the thickest Fe top layer catalyst (sample I) approaches that of the single layer Fe catalyst at about 300 °C. For next thinner top layers (samples J), the temperature increases to 400 °C. Were diffusion limitations not present, the conversion would approach the arithmetic average of the Fe and Cu catalysts, not unlike a mixed layer catalyst.

In conclusion, mass transport limitations cannot be ignored during SCR for moderate to high temperatures and realistic washcoat loadings. This is particularly true for more active catalysts and/or fast SCR conditions. This opens the need for

increasing the gas–solid interfacial area and decreasing the effective washcoat thickness. This may be accomplished through higher density monoliths, for example.

11.5 Reactor Modeling Developments

Progress has been made towards the development of monolith reactor models that predict SCR performance under both steady state and transient operation. Guthenke et al. [33]. provided a thorough review of SCR reactors. Most of the earlier work in this area was done for the more established Vanadia-based catalysts and involved the use of global kinetic models [81–83]. More recent works by Nova et al. provided detailed transient model for the SCR reaction system on Vanadia-based catalyst [8, 45]. Olsson and coworkers developed both global and detailed kinetic models for NH_3-SCR reactions on Cu-ZSM-5 catalysts [14, 15, 49]. More recent works have communicated models for NH_3-SCR reactions on Fe-zeolite catalysts [25, 57, 76, 84].

We highlight in this section some of these more recent developments of reactor models for Fe-based catalysts based on global kinetic descriptions. Our intent is to describe the state of the art, pointing out the main features and limitations of the two recent models. There remains a need to build on the emerging understanding of the mechanistic features of SCR through the use of reactors based on microkinetic models. That will undoubtedly be an area of activity in the coming years [15].

A transient global kinetic model was developed for Fe-exchanged zeolite monolith catalysts by Sjovall et al. [25]. The model incorporates several global reactions involving measured stable species, external mass transfer, and accumulation of adsorbed NH_3. The model treats all reacting and product species as gas phase species except for NH_3 and NH_4NO_3. The model accounts for the known nonideal adsorption and accumulation of NH_3 and assumes that NH_4NO_3 formation and accumulation occurs on a second type of site. In addition to the NH_4NO_3 formation reaction from NO_2 and adsorbed NH_3, the model includes NO oxidation by O_2, standard SCR, fast SCR, and NO_2 SCR. The model does not account for N_2O formation which is known to be a product of NH_4NO_3 decomposition. Instead the NH_4NO_3 is assumed to decompose to NO_2, O_2, and H_2O. The authors modify the stoichiometry of the standard SCR reaction to account for documented "overconsumption" of NH_3 in the presence of NO. In accounting for the coverage of NH_3, the model considers that rate of the standard SCR reaction is proportional to the fraction of vacant sites, so as a result the model predicts the known rate inhibition NH_3. The model does not account for a similar inhibitory effect of NH_3 on the fast SCR chemistry as we have described earlier, however. Finally, the model does not consider the existence of washcoat diffusion limitations which are undoubtedly present above 250 °C when NO_2 is in the feed, or 300 °C during standard SCR. Thus, application of the model to other catalysts would require modification of the kinetic parameters.

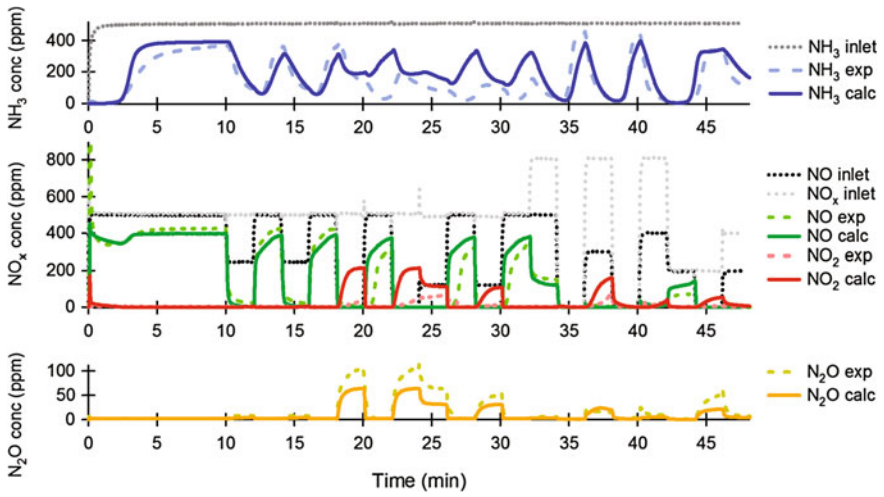

Fig. 11.19 Experimental and model-predicted effluent species concentrations during transient SCR (Used with permission [25].)

The Sjovall et al. [25]. global model was tuned (i.e., parameters estimated) for a systematic and sequential set of experiments spanning NH_3 TPD, NO and NH_3 oxidation, standard SCR, fast SCR, and NO_2 SCR. The model was then validated by its ability to predict SCR for NO_2/NOx feed ratios other than the ones used to tune the model ($\sim$0, 0.5, 0.75). The results of the simulations, which considered both steady-state and transient experiments, reveal good agreement (Fig. 11.19). The transient predictions are especially noteworthy, showing how the catalyst responds to time-varying feeds containing different ratios of NO and NO_2.

Another recent model by Colombo et al. [57]. considered standard, fast, and NO_2 SCR on Fe-exchanged zeolites. This model builds off earlier models for vanadia and Fe catalysts, the new feature being inclusion of NO_2/NOx $\rightarrow$ 1 SCR chemistry. The model includes nonideal isotherm treatment of NH_3 adsorption to predict the ammonia coverage, rate expressions for NO oxidation, NH_3 oxidation, standard SCR (low and low temperature), ammonium nitrate formation and sublimation, N_2O formation, fast SCR, and N_2O formation and consumption. Some specific features are incorporated into rate expressions to account for certain effects. A Mars–Van Krevelen rate expression that includes NH_3 site blocking is used. The model predicts many of the trends in data obtained for commercial Fe-exchanged monolith catalyst (Fig. 11.20). Validation was demonstrated through simulations of NO_2/NOx = 0.25 and 0.75 feeds. Very good agreement was demonstrated between model and experiment. This was described in the study by Guthenke et al. [33] in which the intrinsic kinetics were incorporated into a 1 + 1 D monolith model.

The recently developed SCR reactor model reported by Metkar et al. [76] also utilized a global kinetic description. The reactor and kinetic models have similar features to the Sjovall et al. model but with some added features. Similarities included the incorporation of the key overall reactions and NH_3 adsorption.

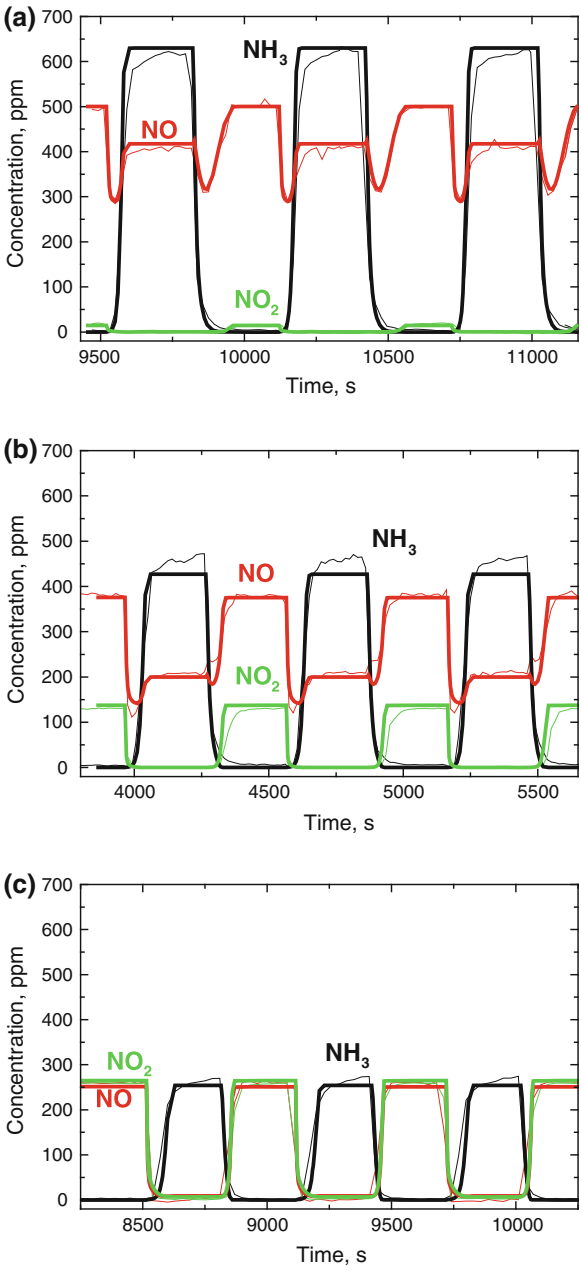

Fig. 11.20 Experimental and model-predicted effluent species concentrations during transient SCR with three different feed concentrations. **a** NO = 500 ppm; **b** NO = 375 ppm, NO^2 = 125 ppm; **c** NO = NO_2 = 250 ppm (Used with permission [57].)

In contrast to the Sjovall et al. model, the Metkar et al. model considered only steady-state data, but accounted for N_2O formation and consumption as well as washcoat diffusion. Specifically, the model accounted for NH_3 adsorption, NH_3

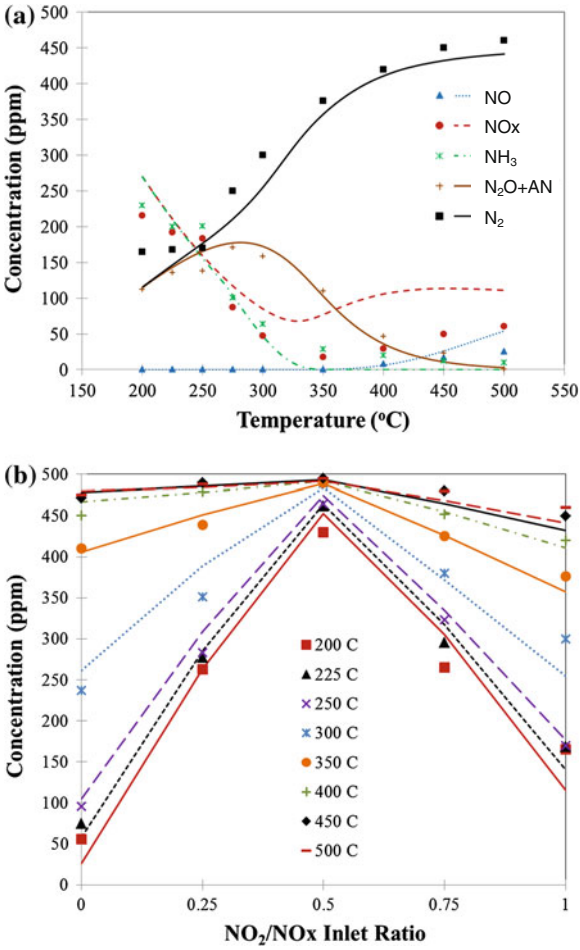

Fig. 11.21 Comparison of experimental (*symbols*) and model-predicted (*lines*) steady-state concentrations of various species obtained during the NO_2 SCR reaction studies carried out on Fe-ZSM-5. Feed: 500 ppm NO_2, 500 ppm NH_3, 5 % O_2, 2 % H_2O. (Adapted from Metkar et al. [76] and used with permission.)

oxidation, NO oxidation, standard SCR, fast SCR, NO_2 SCR, ammonium nitrate formation and its decomposition to N_2O, N_2O decomposition, and N_2O reduction by NH_3. The study also included a global kinetic model for the commercial Cu/chabazite zeolite catalyst commercialized by BASF Inc. This enabled the investigators to simulate combined Fe–Cu catalyst in the sequential brick and dual layer architectures.

The Metkar et al. [76] study followed a similar approach to that of Sjovall et al. [25], utilizing a systematic set of experiments with increasingly complex feeds to estimate parameters. The model was validated by simulating monoliths of different lengths and feeds with different compositions. The model captured very well the NOx and NH_3 conversions and reasonably well the selectivity to the N_2O by-product. An example comparison of model and experiment is shown in Fig. 11.21a. It is interesting to note that the model predicted the onset of washcoat

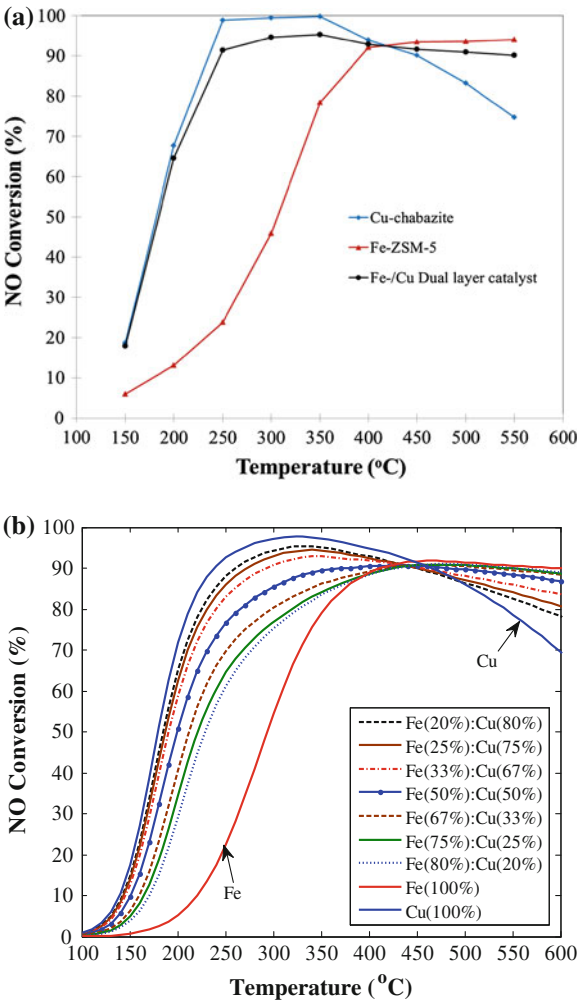

Fig. 11.22 Steady-state NO conversions obtained during the standard SCR reaction on combined Cu- and Fe-exchanged zeolites. The dual layer catalysts for the experiments **a** comprised Fe-ZSM-5 (10–12 wt.%) on the underlying Cu-CHA commercial catalyst. The modeling **b** considered Fe-ZSM-5 as the top layer and Cu-CHA as the bottom layer. (Adapted from Metkar et al. [76] and used with permission.)

diffusion limitations reported in an earlier study. The capability of the model to predict trends over a wide range of temperature and feed compositions is shown in Fig. 11.21b. The model captures most of the overall and specific trends, such as the strong sensitivity to NO_2 at lower temperatures and the existence of the maximum N_2 yield at a NO:NO_2 feed ratio of unity, among other features.

The Metkar et al. [76] model was also used to predict the performance of combined Fe- and Cu-zeolite monolithic catalysts in the form of either sequential bricks or dual layers. Without any adjustment of the kinetic parameters from the tuning of the single component catalysts, the model predicted all of the main trends in the combined system data. An example result is shown in Fig. 11.22. The model predicts the wide expansion in the temperature window giving a high conversion

when the Fe-zeolite monolith was positioned upstream of the Cu-zeolite monolith, or was the top layer of a dual layer monolith. It is important to note that the simulation of the dual layer catalysts would not have been possible without accounting for the internal diffusion of reacting species in the washcoat layer(s). The model confirmed that there exists an optimal loading of Fe-zeolite in the form of a separate monolith brick or top layer. Current work in our group reveals an interesting interplay of reaction and diffusion, enabling the determination of which architecture is best in terms of NOx conversion over a range of temperatures.

11.6 Concluding Remarks

The development of metal-exchange zeolites for lean NOx reduction is one of the more significant developments in catalysis in recent years. In this chapter, we have attempted to capture the latest understanding of Fe-zeolite catalysts in terms of catalyst performance, mechanism, kinetics, reaction-transport interactions, and their combination with Cu-exchanged zeolites in multi-component Fe/Cu monolith catalysts.

The role of kinetic and reactor modeling is crucial in the continued advancement of these catalysts as they are optimized for specific applications. We have described different mechanisms for SCR for feed compositions spanning the standard to fast to NO_2 types. Convergence to the correct mechanisms is essential if predictive mechanistic-based kinetic models are to be developed. To date the kinetic models have been of the global variety. While these are useful for reactor optimization, microkinetic models are needed to guide rational catalyst design and the discovery of new catalyst formulations.

Finally, certain aspects that have not been covered in this chapter include coupled NH_3 and hydrocarbon SCR and SCR catalyst poisoning and aging/deactivation. Understanding and hopefully predicting the useful life of these catalysts is paramount. A molecular-level understanding of the mechanisms of hydrocarbon and sulfur poisoning and thermal degradation relies on mechanistic-based kinetic models.

Acknowledgments The authors wish to thank the U.S. Department of Energy Office of Vehicle Technologies for their support of our research in diesel emissions reduction using SCR. We also acknowledge the fruitful collaborations over the course of several years with Vemuri Balakotaiah (UH) and the helpful discussions with Bill Epling (UH), Krishna Kamasamudram (Cummins Inc.), and Enrico Tronconi (Politecnico di Milano).

References

1. G. Madia, M. Elsener, M. Koebel, F. Raimondi, a Wokaun, Applied Catalysis B: Environmental 39 (2002) 181.
2. C. Ciardelli, I. Nova, E. Tronconi, D. Chatterjee, B. Bandl-Konrad, M. Weibel, B. Krutzsch, Applied Catalysis B: Environmental 70 (2007) 80.
3. M. Koebel, M. Elsener, G. Madia, Industrial & Engineering Chemistry Research 40 (2001) 52.
4. G. Madia, M. Koebel, M. Elsener, A. Wokaun, Industrial & Engineering Chemistry Research 41 (2002) 4008.
5. I. Nova, C. Ciardelli, E. Tronconi, D. Chatterjee, B. Bandl-Konrad, Catalysis Today 114 (2006) 3.
6. M. Koebel, G. Madia, M. Elsener, Catalysis Today 73 (2002) 239.
7. E. Tronconi, I. Nova, C. Ciardelli, D. Chatterjee, B. Bandl-Konrad, T. Burkhardt, Catalysis Today 105 (2005) 529.
8. I. Nova, C. Ciardelli, E. Tronconi, D. Chimica, I. Chimica, P. Milano, I.- Milan, D. Chatterjee, B. Bandl-konrad, D. Ag, A. Rbp, D.- Stuttgart, AIChE Journal 52 (2006).
9. D. Chatterjee, P. Kočí, V. Schmeißer, M. Marek, M. Weibel, B. Krutzsch, Catalysis Today 151 (2010) 395.
10. K. Kamasamudram, N.W. Currier, X. Chen, A. Yezerets, Catalysis Today 151 (2010) 212.
11. K. Kamasamudram, N.W. Currier, T. Szailer, A. Yezerets, SAE International (2010).
12. M. Colombo, I. Nova, E. Tronconi, Catalysis Today 151 (2010) 223.
13. H. Sjövall, L. Olsson, E. Fridell, R.J. Blint, Applied Catalysis B: Environmental 64 (2006) 180.
14. L. Olsson, H. Sjövall, R.J. Blint, Applied Catalysis B: Environmental 81 (2008) 203.
15. H. Sjövall, R.J. Blint, L. Olsson, Applied Catalysis B: Environmental 92 (2009) 138.
16. G. Delahay, B. Coq, L. Broussous, Applied Catalysis B: Environmental 12 (1997) 49.
17. G. Delahay, S. Kieger, N. Tanchoux, P. Trens, B. Coq, Applied Catalysis B: Environmental 52 (2004) 251.
18. J.H. Baik, S.D. Yim, I.-S. Nam, Y.S. Mok, J.-H. Lee, B.K. Cho, S.H. Oh, Industrial & Engineering Chemistry Research 45 (2006) 5258.
19. A. Grossale, I. Nova, E. Tronconi, Catalysis Letters 130 (2009) 525.
20. R. Long, Journal of Catalysis 207 (2002) 224.
21. M. Schwidder, S. Heikens, a Detoni, S. Geisler, M. Berndt, a Bruckner, W. Grunert, Journal of Catalysis 259 (2008) 96.
22. Q. Sun, Z. Gao, H. Chen, W. Sachtler, Journal of Catalysis 201 (2001) 88.
23. M. Devadas, O. Krocher, M. Elsener, a Wokaun, N. Soger, M. Pfeifer, Y. Demel, L. Mussmann, Applied Catalysis B: Environmental 67 (2006) 187.
24. O. Kröcher, M. Devadas, M. Elsener, A. Wokaun, N. Söger, M. Pfeifer, Y. Demel, L. Mussmann, Applied Catalysis B: Environmental 66 (2006) 208.
25. H. Sjovall, R.J. Blint, A. Gopinath, L. Olsson, Industrial & Engineering Chemistry Research 49 (2010) 39.
26. M. Iwasaki, K. Yamazaki, H. Shinjoh, Applied Catalysis A: General 366 (2009) 84.
27. A. Grossale, I. Nova, E. Tronconi, D. Chatterjee, M. Weibel, Journal of Catalysis 256 (2008) 312.
28. S. Zones, Zeolite SSZ-13 and Its Method of Preparation, U.S. Patent US4544538, 1985.
29. I. Bull, W.-M. Xue, P. Burk, R.S. Boorse, W.M. Jaglowski, G.S. Koermer, A. Moini, J.A. Patchett, J.C. Dettling, M.T. Caudle, Copper CHA Zeolite Catalysts, U.S. Patent US7601662, 2009.
30. S.J. Schmieg, S.H. Oh, C.H. Kim, D.B. Brown, J.H. Lee, C.H.F. Peden, D.H. Kim, Catalysis Today 184 (2012) 252.
31. H.-X. Li, W.E. Cormier, B. Moden, Novel Microporous Crystalline Material Comprising a Molecular Sieve, U.S. Patent US 2008/0241060 A1, 2010.
32. S. Brandenberger, O. Kröcher, A. Tissler, R. Althoff, Catalysis Reviews 50 (2008) 492.

33. A. Guthenke, D. Chatterjee, M. Weibel, B. Krutzsch, P. Koci, I. Nova, E. Tronconi, Advances in Chemical Engineering 33 (2008) 103.
34. M. Devadas, O. Krocher, M. Elsener, a Wokaun, N. Soger, M. Pfeifer, Y. Demel, L. Mussmann, Applied Catalysis B: Environmental 67 (2006) 187.
35. H.Y. Huang, R.Q. Long, R.T. Yang, Applied Catalysis A: General 235 (2002) 241.
36. A. Grossale, I. Nova, E. Tronconi, Catalysis Today 136 (2008) 18.
37. H.-Y. Chen, T. Voskoboinikov, W.M.H. Sachtler, Journal of Catalysis 186 (1999) 91.
38. M. Iwasaki, K. Yamazaki, K. Banno, H. Shinjoh, Journal of Catalysis 260 (2008) 205.
39. M. Devadas, O. Krocher, a Wokaun, Reaction Kinetics and Catalysis Letters 86 (2005) 347.
40. A. Grossale, I. Nova, E. Tronconi, Journal of Catalysis 265 (2009) 141.
41. G. Delahay, D. Valade, a Guzmanvargas, B. Coq, Applied Catalysis B: Environmental 55 (2005) 149.
42. P.S. Metkar, N. Salazar, R. Muncrief, V. Balakotaiah, M.P. Harold, Applied Catalysis B: Environmental 104 (2011) 110.
43. M. Koebel, Journal of Catalysis 209 (2002) 159.
44. I. Nova, C. Ciardelli, E. Tronconi, D. Chatterjee, M. Weibel, Topics in Catalysis 42-43 (2007) 43.
45. I. Nova, C. Ciardelli, E. Tronconi, D. Chatterjee, M. Weibel, AIChE Journal 55 (2009) 1514.
46. Y.H. Yeom, B. Wen, W.M.H. Sachtler, E. Weitz, Journal of Physical Chemistry B 108 (2004) 5386.
47. Y. Yeom, M. Li, A. Savara, W. Sachtler, E. Weitz, Catalysis Today 136 (2008) 55.
48. C. Ciardelli, I. Nova, E. Tronconi, B. Bandl-konrad, Chem. Communications 3264 (2004) 2718.
49. Y. Yeom, J. Henao, M. Li, W. Sachtler, E. Weitz, Journal of Catalysis 231 (2005) 181.
50. S. Suárez, S. Moon, P. Avila, P. Grange, J. Blanco, 75 (2002) 331.
51. J.R. Klovsky, P. Koradla, C.T. Lim, Industrial & Engineering Chemistry Product Research and Development 19 (1980) 218.
52. M. Richter, R. Eckelt, B. Parlitz, R. Fricke, Applied Catalysis B: Environmental 15 (1998) 129.
53. L. Olsson, H. Sjövall, R.J. Blint, Applied Catalysis B: Environmental 87 (2009) 200.
54. M.P. Ruggeri, I. Nova, E. Tronconi, in:, CAPoC9, Brussels, 2012.
55. D. Bhatia, R.W. McCabe, M.P. Harold, V. Balakotaiah, Journal of Catalysis 266 (2009) 106.
56. P.S. Metkar, V. Balakotaiah, M.P. Harold, Catalysis Today 184 (2012) 115.
57. M. Colombo, I. Nova, E. Tronconi, V. Schmeißer, B. Bandl-Konrad, L. Zimmermann, Applied Catalysis B: Environmental 111-112 (2012) 106.
58. A. Grossale, I. Nova, E. Tronconi, D. Chatterjee, M. Weibel, Topics in Catalysis 52 (2009) 1837.
59. P.S. Metkar, V. Balakotaiah, M.P. Harold, Catalysis Today 184 (2012) 115.
60. J. Eng, C.H. Bartholomew, Journal of Catalysis 171 (1997) 27.
61. M. Rivallan, G. Ricchiardi, S. Bordiga, A. Zecchina, Journal of Catalysis 264 (2009) 104.
62. J.M. Fedeyko, B. Chen, H.-Y. Chen, Catalysis Today 151 (2010) 231.
63. M. Iwasaki, H. Shinjoh, Journal of Catalysis 273 (2010) 29.
64. M. Li, Y. Yeom, E. Weitz, W. Sachtler, Journal of Catalysis 235 (2005) 201.
65. C.H. Bibart, G.E. Ewing, The Journal of Chemical Physics 61 (1974) 1293.
66. M. Ahrens, O. Marie, P. Bazin, M. Daturi, Journal of Catalysis 271 (2010) 1.
67. M.E. Jenkin, O.X. Ora, Atmospheric Environment 22 (1987) 487.
68. M.W. Ross, T.C. DeVore, The Journal of Physical Chemistry. A 112 (2008) 6609.
69. R. Kefirov, E. Ivanova, K. Hadjiivanov, S. Dzwigaj, M. Che, Catalysis Letters 125 (2008) 209.
70. G. Panov, E. Starokon, L. Pirutko, E. Paukshtis, V. Parmon, Journal of Catalysis 254 (2008) 110.
71. Q. Sun, Z. Gao, B. Wen, W.M.H. Sachtler, Catalysis Letters 78 (2002) 3.
72. Y. Kameoka, R.L. Pigford, Industrial & Engineering Chemistry Research 16 (1977) 163.

73. B.R. Kromer, L. Cao, L. Cumaranatunge, S.S. Mulla, J.L. Ratts, A. Yezerets, N.W. Currier, F.H. Ribeiro, W.N. Delgass, J.M. Caruthers, Catalysis Today 136 (2008) 93.
74. S. Brandenberger, O. Kröcher, A. Tissler, R. Althoff, Applied Catalysis B: Environmental 95 (2010) 348.
75. M. Li, J. Henao, Y. Yeom, E. Weitz, W.M.H. Sachtler, Catalysis Letters 98 (2004) 5.
76. P.S. Metkar, M.P. Harold, V. Balakotaiah, Chemical Engineering Science 87 (2013) 51.
77. M.P. Ruggeri, A. Grossale, I. Nova, E. Tronconi, H. Jirglova, Z. Sobalik, Catalysis Today 184 (2012) 107.
78. P.S. Metkar, V. Balakotaiah, M.P. Harold, Chemical Engineering Science 66 (2011) 5192.
79. I. Nova, D. Bounechada, R. Maestri, E. Tronconi, A.K. Heibel, T.A. Collins, T. Boger, Industrial & Engineering Chemsitry Research 50 (2011) 299.
80. P.S. Metkar, M.P. Harold, V. Balakotaiah, Applied Catalysis B: Environmental 111-112 (2012) 67.
81. J.A. Dumesic, N. Topsøe, H. Topsøe, Y. Chen, T. Slabiak, 417 (1996) 409.
82. B. Roduit, A. Wokaun, A. Baiker, Industrial & Engineering Chemistry Research 37 (2000) 4577.
83. R. Willi, B. Roduit, R.A. Koeppel, A. Wokaun, I. Chemistry, Chemical Engineering Science 51 (2000) 2897.
84. S. Malmberg, M. Votsmeier, J. Gieshoff, N. Söger, L. Mußmann, a. Schuler, a. Drochner, Topics in Catalysis 42-43 (2007) 33.